CSIAM Trans. Appl. Math.
doi: 10.4208/csiam-am.SO-2024-0067

Vol. **x**, No. x, pp. 1-31
xx 2025

Linear Maximum Bound Principle Preserving Finite Difference Schemes for the Convective Allen-Cahn Equation

Jingwei Li[1], Kun Wang[2,*] and Lili Ju[3]

[1] *School of Mathematics and Statistic, Lanzhou University, Lanzhou 730000, China.*
[2] *College of Mathematics and Statistics, Chongqing University, Chongqing 401331, China.*
[3] *Department of Mathematics, University of South Carolina, Columbia, SC 29208, USA.*

Received 20 December 2024; Accepted 8 August 2025

Abstract. The convective Allen-Cahn equation generalizes the classical Allen-Cahn equation by introducing an additional convective term associated with a solenoidal velocity field while maintaining the maximum bound principle (MBP). However, developing high-order numerical schemes that are accurate in both time and space and preserve the MBP unconditionally has remained a significant challenge. In this paper, we address this by first defining new auxiliary variables to reformulate the interaction of the velocity field with the phase field. We then transform the convective Allen-Cahn equation into a generalized Fokker-Planck form using an exponential transformation, enabling the development of MBP-preserving linear numerical schemes. Subsequently, we propose first- and second-order in time numerical schemes for the reformulated equations with a second-order quasi-symmetric finite difference discretization in space. In this approach, the auxiliary variables are replaced with known functions related to the velocity field, simplifying the numerical implementation. For the first-order in time scheme, we derive its optimal error estimate and prove its unconditional MBP-preservation. For the second-order in time scheme, we show its MBP-preservation under mild constraints on the mesh and time step sizes. Some numerical experiments in two and three dimensions are also presented to validate the theoretical findings and illustrate the accuracy and efficiency of our proposed schemes.

AMS subject classifications: 35B50, 35K55, 65M12, 65R20

Key words: Convective Allen-Cahn equation, maximum bound principle, exponential transformation, quasi-symmetric finite difference, error estimation.

*Corresponding author. *Email addresses:* lijingwei@lzu.edu.cn (J. Li), kunwang@cqu.edu.cn (K. Wang), ju@math.sc.edu (L. Ju)

1 Introduction

In this paper, we consider the convective Allen-Cahn equation in the following form:

$$u_t+\mathbf{v}\cdot\nabla u=\Delta u+\frac{f(u)}{\epsilon^2},\quad t\in(0,T],\quad \mathbf{x}\in\Omega,$$

where $\Omega\subset\mathbb{R}^d$ $(d=2,3)$ is a connected, open, and bounded domain. Here, $T>0$ is the terminal time, $u(\mathbf{x},t)\in\mathbb{R}$ is the phase variable, and $\mathbf{v}(\mathbf{x},t)=(v_1(\mathbf{x},t),v_2(\mathbf{x},t),\ldots,v_d(\mathbf{x},t))^\top\in\mathbb{R}^d$ is the fluid velocity, satisfying the divergence-free condition $\nabla\cdot\mathbf{v}=0$ for $t\in(0,T]$ and $\mathbf{x}\in\Omega$. The interface parameter ϵ determines the thickness of the transition layers, and the reaction term $f=-F'$, where $F(u)$ represents the bulk potential function. If the velocity field $\mathbf{v}$ vanishes, the convective Allen-Cahn equation reduces to the classical Allen-Cahn equation (see, e.g. [1, 2, 27, 47])

$$u_t=\Delta u+\frac{f(u)}{\epsilon^2},$$

which is widely used to model phenomena such as mean curvature flow [16] and image segmentation [17]. The classic Allen-Cahn equation can also be viewed as the gradient flow corresponding to the free energy functional

$$E(u)=\int_\Omega\frac{1}{2}|\nabla u|^2+\frac{F(u)}{\epsilon^2}\mathrm{d}\mathbf{x}. \tag{1.1}$$

Under periodic or homogeneous Neumann boundary conditions, it is straightforward to verify that the classical Allen-Cahn equation dissipates the energy $E(u)$, satisfying $dE(u)/dt=-\int_\Omega|u_t|^2\mathrm{d}\mathbf{x}\le 0$. In contrast, the convective Allen-Cahn equation is more complex due to the convective term involving the velocity field. While the energy dissipation law is generally not preserved, even with a divergence-free velocity, the convective Allen-Cahn equation retains the maximum bound principle. This implies that the solution to the time-dependent equation remains bounded by a specific constant in the absolute norm for all times [13].

The MBP is a critical physical property of the phase field, playing a central role in numerical simulations. Considerable efforts have been made to design MBP-preserving numerical methods. For the classical Allen-Cahn equation, these include mass-lumping finite element methods [50, 51], finite difference methods [4, 49], and finite volume methods [42] for spatial discretization. Time integration techniques include first-order stabilized linear semi-implicit schemes and higher-order schemes [25, 30, 33, 48, 53, 54]. For the time-fractional Allen-Cahn equation, MBP-preserving schemes include linear and nonlinear Crank-Nicolson methods [21, 22] and second-order backward differentiation formula (BDF) methods with variable time steps [8, 34–36]. Moreover, MBP-preserving schemes have been developed for other Allen-Cahn-type equations, such as stabilized exponential time differencing schemes for the nonlocal Allen-Cahn equation [12] and the conservative Allen-Cahn equation [24, 32].

The convective term poses additional challenges in designing MBP-preserving schemes for the convective Allen-Cahn equation. Among various approaches, the upwinding scheme is popular due to its ability to form an M-matrix, which aids in MBP preserva-

tion. For example, Shen *et al.* [44] proposed a stabilized semi-implicit scheme, while Cai *et al.* [4] employed the exponential time differencing scheme. Then Du and Hou [14] presented a stabilized Crank-Nicolson scheme. Though these schemes unconditionally preserve the MBP, they are only first-order accurate in space, as higher-order schemes typically fail to form an M-matrix. High-order spatial accuracy is often essential for capturing interface dynamics in scenarios where convection dominates, especially when the interface width is small. To address this, operator splitting methods have gained traction, achieving higher-order spatial accuracy while preserving the MBP. Examples include the weighted essentially non-oscillatory (WENO) scheme with an MBP-preserving limiter [29] and the semi-Lagrangian scheme with cut-off post-processing [31]. Other MBP-preserving techniques have been explored as well, e.g. [46], though these higher-order methods often impose strict Courant-Friedrichs-Lewy (CFL) stability conditions.

In this work, we first introduce new auxiliary variables to reformulate the convective Allen-Cahn equation, which unifies the diffusion and convection terms into a single term involving a self-adjoint elliptic operator via an exponential transformation. Together with a second-order quasi-symmetric finite difference discretization in space, we propose first- and second-order in time linear numerical schemes for full discretization of the reformulated equation (i.e. a generalized Fokker-Planck form). The exponential factor is replaced with known functions related to the velocity field, simplifying the numerical implementation. We show that the proposed schemes guarantee MBP preservation under mild constraints on the mesh and time step sizes. Moreover, they achieve second-order spatial accuracy while only solving linear equations at each time step. The primary contributions of this paper are as follows: 1) We reformulate the diffusion and convection terms into a single term involving a self-adjoint elliptic operator via an exponential transformation, enabling the construction of MBP-preserving schemes with second-order spatial accuracy; 2) By replacing the auxiliary variables with known functions related to the velocity field, we simplify the computational implementation; 3) We provide a detailed analysis of the discrete MBP stability and convergence properties of the proposed schemes.

The rest of the paper is organized as follows. Section 2 briefly reviews the MBP and derives the equivalent form of the convective Allen-Cahn equation. Section 3 presents the first-order in time scheme and corresponding MBP and fully discrete error analysis. Section 4 gives the second-order in time scheme and corresponding MBP analysis. In Section 5, through numerical experiments we validate the theoretical results and demonstrate the performance of the proposed schemes. Finally, some remarks are concluded in Section 6.

2 Maximum bound principle, equivalent form and discrete differential operators

In this section, we first recall the MBP of the convective Allen-Cahn equation, then deduce an equivalent form of the equation via an exponential transformation, which is

a generalized Fokker-Planck equation and plays an essential role in constructing the MBP-preserving numerical schemes. In addition, some discrete differential operators by finite difference in space are reviewed.

2.1 Maximum bound principle

In this subsection, we briefly review the conditions for the MBP in the context of the convective Allen-Cahn equation. We start by considering the convective Allen-Cahn equation

$$u_t = \Delta u - \mathbf{v}\cdot\nabla u + f^{\epsilon}(u), \quad t\in(0,T], \quad \mathbf{x}\in\Omega, \tag{2.1}$$

where $\nabla\cdot\mathbf{v}=0$, $f^{\epsilon}(u)=f(u)/\epsilon^2$, and the initial value is given by

$$u(\mathbf{x},0)=u_0(\mathbf{x}), \quad \mathbf{x}\in\overline{\Omega}. \tag{2.2}$$

Here, $f(u)$ is assumed to be continuously differentiable with respect to u. For simplicity, we impose periodic boundary conditions (for a rectangular domain $\Omega=\Pi_{i=1}^{d}(a_i,b_i)$). The extension to homogeneous Neumann boundary conditions is straightforward. To establish the MBP property for the convective Allen-Cahn equation, the following assumption on the nonlinear function $f(u)$ is required.

Assumption 2.1 ([13,33]). There exists a constant $\beta>0$ such that

$$f(\beta)\le 0\le f(-\beta).$$

Two widely-used potential functions that satisfy Assumption 2.1 are of particular interest in the phase-field model. The first is the double-well potential, given by

$$F(u)=\frac{1}{4}(1-u^2)^2, \quad f(u)=-F'(u)=u-u^3 \tag{2.3}$$

with the bounding constant $\beta\in[1,+\infty]$. The second is the Flory-Huggins potential, given by

$$\begin{aligned} F(u)&=\frac{\theta}{2}[(1+u)\ln(1+u)+(1-u)\ln(1-u)]-\frac{\theta_c}{2}u^2,\\ f(u)&=-F'(u)=\frac{\theta}{2}\ln\frac{1-u}{1+u}+\theta_c u, \end{aligned} \tag{2.4}$$

where $\theta_c>\theta>0$, and the bounding constant $\beta\in[\eta,1)$ with η being the positive root of $f(\eta)=0$.

Using the supremum norm $|\cdot|_\infty$ on $C(\overline{\Omega})$, one can show that the convective Allen-Cahn equation (2.1) with the initial value (2.2) and either potential function (2.3) or (2.4) admits a unique MBP solution. This leads to the following theorem.

Theorem 2.1 ([15,29]). *Suppose Assumption* 2.1 *is satisfied, and*

$$\mathbf{v}\in C\big(0,T;C^1(\Omega)^d\big)\cap C\big(0,T;C(\bar{\Omega})^d\big).$$

Assume $u\in C^1(0,T;C^2(\Omega))\cap C(0,T;C^1(\overline{\Omega}))$ *is a solution to the problem* (2.1)-(2.2). *If the initial value satisfies* $|u_0|_\infty\le\beta$, *then* $|u(\cdot,t)|_\infty\le\beta$ *for all* $t\in[0,T]$.

2.2 Equivalent form

Next, we derive an equivalent form of the convective Allen-Cahn equation (2.1), which is essential for constructing an MBP-preserving scheme. Using the condition $\nabla\cdot\mathbf{v}=0$, Eq. (2.1) can be rewritten as

$$u_t=\Delta u-\nabla\cdot(\mathbf{v}u)+f^\epsilon(u)=\nabla\cdot(\nabla u-\mathbf{v}u)+f^\epsilon(u). \tag{2.5}$$

For simplicity, here we consider the two dimensional problem for illustration, i.e. $d=2$ and $\mathbf{x}=(x,y)$. Note that all algorithms and analysis presented below can be naturally extended to non-tensor domains and three dimensions. For any given point $(x^0,y^0)\in\overline{\Omega}$, define the auxiliary variables

$$w_1(x,y,t)=\int_{x^0}^{x}v_1(s,y,t)\mathrm{d}s,\quad w_2(x,y,t)=\int_{y^0}^{y}v_2(x,r,t)\mathrm{d}r.$$

Then, the following transformations hold:

$$u_x-v_1u=e^{w_1(x,y,t)}(e^{-w_1(x,y,t)}u)_x,\quad u_y-v_2u=e^{w_2(x,y,t)}(e^{-w_2(x,y,t)}u)_y, \tag{2.6}$$

which, combined with (2.5), yields an equivalent form of the convection Allen-Cahn equation (2.1)

$$u_t=\left(e^{w_1(x,y,t)}(e^{-w_1(x,y,t)}u)_x\right)_x+\left(e^{w_2(x,y,t)}(e^{-w_2(x,y,t)}u)_y\right)_y+f^\epsilon(u), \tag{2.7}$$

subject to the initial condition (2.2).

Here, $e^{-w_1}u$ and $e^{-w_2}u$ are considered generalized Slotboom variables. The resulting elliptic operator is of a generalized Fokker-Planck form and can be discretized with symmetrical fluxes, often yielding a mass-conservative and positivity-preserving scheme [26, 38, 39]. Through (2.7), the diffusion and convection terms in (2.5) are reformulated into a term involving a self-adjoint elliptic operator via the exponential transformation (2.6) applied to the flux $\nabla u-\mathbf{v}u$. In the following, we will take the equivalent form (2.7) to develop MBP-preserving schemes for the convective Allen-Cahn equation (2.1).

2.3 Discrete differential operators in space

Assume the domain $\Omega=(0,L_x)\times(0,L_y)$, where for simplicity, we assume $L_x=L_y=L$. Let $h=L/N$ $(N\in\mathbb{Z}^+)$ be the mesh size, the uniform partition Ω_h of the domain Ω is

$$\Omega_h=\{(x_i,y_j)\,|\,x_i=ih,y_j=jh,0\le i,j\le N\}$$

with the periodic grid function spaces

$$\mathcal{C}:=\{u\,|\,u_{i,j}=u_{i\pm N,j\pm N},\forall i,j=1,2,\ldots,N\}.$$

The average and difference operators can be defined as

$$a_x u_{i,j} = \frac{u_{i+1/2,j} + u_{i-1/2,j}}{2}, \quad a_y u_{i,j} = \frac{u_{i,j+1/2} + u_{i,j-1/2}}{2},$$
$$d_x u_{i,j} = \frac{u_{i+1/2,j} - u_{i-1/2,j}}{h}, \quad d_y u_{i,j} = \frac{u_{i,j+1/2} - u_{i,j-1/2}}{h}.$$

Then, for grid functions $u,v \in \mathcal{C}$, the discrete gradient and discrete divergence operators can be denoted by

$$\nabla_h u_{i,j} = \left(d_x u_{i+\frac{1}{2},j}, d_y u_{i,j+\frac{1}{2}}\right), \quad \nabla_h \cdot (u,v)_{i,j} = d_x u_{i,j} + d_y v_{i,j},$$

and the discrete Laplacian Δ_h can be given by

$$\begin{aligned}\Delta_h u_{i,j} &= \nabla_h \cdot (\nabla_h u)_{i,j} = d_x (d_x u)_{i,j} + d_y (d_y u)_{i,j} \\ &= \frac{1}{h^2}(u_{i+1,j} + u_{i-1,j} + u_{i,j+1} + u_{i,j-1} - 4u_{i,j}).\end{aligned}$$

Moreover, if $\mathcal{D}$ is a scalar function defined at the central point, we have

$$\nabla_h \cdot (\mathcal{D} \nabla_h u)_{i,j} = d_x (\mathcal{D} d_x u)_{i,j} + d_y (\mathcal{D} d_y u)_{i,j}. \tag{2.8}$$

Obviously, the above discrete operators are all second-order approximations of the corresponding differential operators.

We also recall the discrete L^2 inner product $\langle u,v \rangle_h = h^2 \sum_{i,j=1}^N u_{i,j} v_{i,j}$ with the induced norm $\|u\|_h = \langle u,u \rangle_h^{1/2}$, the discrete H^1 inner product

$$\langle \nabla_h u, \nabla_h v \rangle_h = h^2 \sum_{i,j=1}^N \left(d_x u_{i-\frac{1}{2},j} d_x v_{i-\frac{1}{2},j} + d_y u_{i,j-\frac{1}{2}} d_y v_{i,j-\frac{1}{2}}\right)$$

with the induced norm $\|\nabla_h u\|_h = \langle \nabla_h u, \nabla_h u \rangle_h^{1/2}$ and the infinity norm

$$\|u\|_\infty := \max_{1 \le i,j \le N} |u_{i,j}|.$$

3 The first- and second-order numerical scheme in time and space

Let $\tau = T/M$ $(M \in \mathbb{Z}^+)$ be a uniform time step and $t_n = n\tau$ $(n = 0,1,2,\ldots,M)$. Denote by $\mathcal{I}_h$ the interpolation operator pointwisely limiting some continuous functions into Ω_h and $u_{i,j}^n$ the discrete approximation of $u(x_i,y_j,t_n)$. Applying the harmonic mean to approximate the self-adjoint elliptic operator in space, and utilizing the implicit and explicit treatments for the linear and nonlinear terms of (2.7) in time respectively, we get

a first-order in time semi-implicit fully discrete scheme for (2.7) as follows: Given $u^0 = \mathcal{I}_h u_0(\mathbf{x}) \in \mathcal{C}$, for $n = 0,1,\ldots,M-1$ find $u^{n+1} \in \mathcal{C}$ such that

$$\frac{u^{n+1}-u^n}{\tau} = \mathcal{Q}_h^{n+1}u^{n+1} - \frac{\kappa}{\epsilon^2}u^{n+1} + f_\kappa^\epsilon(u^n) \tag{3.1}$$

with $f_\kappa^\epsilon(u) = f^\epsilon(u) + (\kappa/\epsilon^2)u$ and

$$\begin{aligned}\mathcal{Q}_h^{n+1}u_{i,j}^{n+1} &= d_x\left(\overline{e^{w_1^{n+1}}}d_x\left(e^{-w_1^{n+1}}u^{n+1}\right)\right)_{i,j} + d_y\left(\overline{e^{w_2^{n+1}}}d_y\left(e^{-w_2^{n+1}}u^{n+1}\right)\right)_{i,j}\\ &= \frac{1}{h}\left(J_{i+\frac{1}{2},j}^{n+1} - J_{i-\frac{1}{2},j}^{n+1}\right) + \frac{1}{h}\left(J_{i,j+\frac{1}{2}}^{n+1} - J_{i,j-\frac{1}{2}}^{n+1}\right),\end{aligned} \tag{3.2}$$

where $\overline{e^{\phi^{n+1}}}$ is the central point value approximated by the harmonic mean

$$\begin{aligned}\overline{e^{\phi_{i\pm\frac{1}{2},j}^{n+1}}} &= \frac{2e^{\phi_{i\pm1,j}^{n+1}}e^{\phi_{i,j}^{n+1}}}{e^{\phi_{i\pm1,j}^{n+1}}+e^{\phi_{i,j}^{n+1}}} = \left(\frac{e^{-\phi_{i\pm1,j}^{n+1}}+e^{-\phi_{i,j}^{n+1}}}{2}\right)^{-1},\\ \overline{e^{\phi_{i,j\pm\frac{1}{2}}^{n+1}}} &= \frac{2e^{\phi_{i,j\pm1}^{n+1}}e^{\phi_{i,j}^{n+1}}}{e^{\phi_{i,j\pm1}^{n+1}}+e^{\phi_{i,j}^{n+1}}} = \left(\frac{e^{-\phi_{i,j\pm1}^{n+1}}+e^{-\phi_{i,j}^{n+1}}}{2}\right)^{-1}.\end{aligned} \tag{3.3}$$

Here $\kappa > 0$ is a stabilizing parameter required to satisfy

$$\kappa \geq \max_{|\xi|\leq\beta}|f'(\xi)|, \tag{3.4}$$

and the numerical fluxes in (3.2) are given by

$$\begin{aligned}J_{i+\frac{1}{2},j}^{n+1} &= \frac{2}{h}\frac{e^{(w_1)_{i+1,j}^{n+1}}e^{(w_1)_{i,j}^{n+1}}}{e^{(w_1)_{i+1,j}^{n+1}}+e^{(w_1)_{i,j}^{n+1}}}\left(u_{i+1,j}^{n+1}e^{-(w_1)_{i+1,j}^{n+1}} - u_{i,j}^{n+1}e^{-(w_1)_{i,j}^{n+1}}\right)\\ &= \frac{2}{h}\left(\frac{1}{1+e^{(w_1)_{i+1,j}^{n+1}-(w_1)_{i,j}^{n+1}}}u_{i+1,j}^{n+1} - \frac{1}{1+e^{(w_1)_{i,j}^{n+1}-(w_1)_{i+1,j}^{n+1}}}u_{i,j}^{n+1}\right),\end{aligned} \tag{3.5a}$$

$$\begin{aligned}J_{i-\frac{1}{2},j}^{n+1} &= \frac{2}{h}\frac{e^{(w_1)_{i-1,j}^{n+1}}e^{(w_1)_{i,j}^{n+1}}}{e^{(w_1)_{i-1,j}^{n+1}}+e^{(w_1)_{i,j}^{n+1}}}\left(u_{i,j}^{n+1}e^{-(w_1)_{i,j}^{n+1}} - u_{i-1,j}^{n+1}e^{-(w_1)_{i-1,j}^{n+1}}\right)\\ &= \frac{2}{h}\left(\frac{1}{1+e^{(w_1)_{i,j}^{n+1}-(w_1)_{i-1,j}^{n+1}}}u_{i,j}^{n+1} - \frac{1}{1+e^{(w_1)_{i-1,j}^{n+1}-(w_1)_{i,j}^{n+1}}}u_{i-1,j}^{n+1}\right),\end{aligned} \tag{3.5b}$$

$$\begin{aligned}J_{i,j+\frac{1}{2}}^{n+1} &= \frac{2}{h}\frac{e^{(w_2)_{i,j+1}^{n+1}}e^{(w_2)_{i,j}^{n+1}}}{e^{(w_2)_{i,j+1}^{n+1}}+e^{(w_2)_{i,j}^{n+1}}}\left(u_{i,j+1}^{n+1}e^{-(w_2)_{i,j+1}^{n+1}} - u_{i,j}^{n+1}e^{-(w_2)_{i,j}^{n+1}}\right)\\ &= \frac{2}{h}\left(\frac{1}{1+e^{(w_2)_{i,j+1}^{n+1}-(w_2)_{i,j}^{n+1}}}u_{i,j+1}^{n+1} - \frac{1}{1+e^{(w_2)_{i,j}^{n+1}-(w_2)_{i,j+1}^{n+1}}}u_{i,j}^{n+1}\right),\end{aligned} \tag{3.5c}$$

$$J^{n+1}_{i,j-\frac{1}{2}} = \frac{2}{h}\frac{e^{(w_2)^{n+1}_{i,j-1}}e^{(w_2)^{n+1}_{i,j}}}{e^{(w_2)^{n+1}_{i,j-1}}+e^{(w_2)^{n+1}_{i,j}}}\left(u^{n+1}_{i,j}e^{-(w_2)^{n+1}_{i,j}} - u^{n+1}_{i,j-1}e^{-(w_2)^{n+1}_{i,j-1}}\right)$$
$$= \frac{2}{h}\left(\frac{1}{1+e^{(w_2)^{n+1}_{i,j}-(w_2)^{n+1}_{i,j-1}}}u^{n+1}_{i,j} - \frac{1}{1+e^{(w_2)^{n+1}_{i,j-1}-(w_2)^{n+1}_{i,j}}}u^{n+1}_{i,j-1}\right). \tag{3.5d}$$

Due to the introduction of the new auxiliary variables w_1 and w_2 in the proposed scheme above, it is necessary to compute integral equations for v_1 and v_2 when implementing (3.1) directly, which will increase the computational cost. To deal with this issue, we apply the midpoint formula, that is

$$\begin{aligned}
(w_1)^{n+1}_{i+1,j} - (w_1)^{n+1}_{i,j} &= \int_{x_i}^{x_{i+1}} v_1(s,y_j,t_{n+1})\mathrm{d}s \approx h\big(v_1^{n+1}\big)_{i+\frac{1}{2},j},\\
(w_1)^{n+1}_{i,j} - (w_1)^{n+1}_{i-1,j} &= \int_{x_{i-1}}^{x_i} v_1(s,y_j,t_{n+1})\mathrm{d}s \approx h\big(v_1^{n+1}\big)_{i-\frac{1}{2},j},\\
(w_2)^{n+1}_{i,j+1} - (w_2)^{n+1}_{i,j} &= \int_{y_j}^{y_{j+1}} v_2(x_i,r,t_{n+1})\mathrm{d}r \approx h\big(v_2^{n+1}\big)_{i,j+\frac{1}{2}},\\
(w_2)^{n+1}_{i,j} - (w_2)^{n+1}_{i,j-1} &= \int_{y_{j-1}}^{y_j} v_2(x_i,r,t_{n+1})\mathrm{d}r \approx h\big(v_2^{n+1}\big)_{i,j-\frac{1}{2}}.
\end{aligned}$$

Consequently, the numerical fluxes in (3.5) can be approximated by

$$\begin{aligned}
\widetilde{J}^{n+1}_{i+\frac{1}{2},j} &= \frac{2}{h}\left(\frac{u^{n+1}_{i+1,j}}{1+e^{h(v_1^{n+1})_{i+1/2,j}}} - \frac{u^{n+1}_{i,j}}{1+e^{-h(v_1^{n+1})_{i+1/2,j}}}\right),\\
\widetilde{J}^{n+1}_{i-\frac{1}{2},j} &= \frac{2}{h}\left(\frac{u^{n+1}_{i,j}}{1+e^{h(v_1^{n+1})_{i-1/2,j}}} - \frac{u^{n+1}_{i-1,j}}{1+e^{-h(v_1^{n+1})_{i-1/2,j}}}\right),\\
\widetilde{J}^{n+1}_{i,j+\frac{1}{2}} &= \frac{2}{h}\left(\frac{u^{n+1}_{i,j+1}}{1+e^{h(v_2^{n+1})_{i,j+1/2}}} - \frac{u^{n+1}_{i,j}}{1+e^{-h(v_2^{n+1})_{i,j+1/2}}}\right),\\
\widetilde{J}^{n+1}_{i,j-\frac{1}{2}} &= \frac{2}{h}\left(\frac{u^{n+1}_{i,j}}{1+e^{h(v_2^{n+1})_{i,j-1/2}}} - \frac{u^{n+1}_{i,j-1}}{1+e^{-h(v_2^{n+1})_{i,j-1/2}}}\right).
\end{aligned} \tag{3.6}$$

In (3.6), the values of the introduced auxiliary variables w_1 and w_2 in the numerical fluxes are replaced with some known functions with respect to the velocity field $\mathbf{v}$, which allow us avoiding solving the integral equations, significantly simplifying the numerical implementation and improving the computational efficiency.

Finally, we obtain a computable form of the original first-order scheme (3.1) (denoted as the SI scheme) as follows:

$$\frac{u^{n+1}-u^n}{\tau} = \widetilde{\mathcal{Q}}^{n+1}_h u^{n+1} - \frac{\kappa}{\epsilon^2}u^{n+1} + f^{\epsilon}_{\kappa}(u^n), \tag{3.7}$$

where

$$\widetilde{\mathcal{Q}}_h^{n+1}u_{i,j}^{n+1}=\frac{1}{h}\left(\widetilde{J}_{i+\frac{1}{2},j}^{n+1}-\widetilde{J}_{i-\frac{1}{2},j}^{n+1}\right)+\frac{1}{h}\left(\widetilde{J}_{i,j+\frac{1}{2}}^{n+1}-\widetilde{J}_{i,j-\frac{1}{2}}^{n+1}\right) \tag{3.8}$$

with the numerical fluxes defined in (3.6). The SI scheme (3.7) is expected to be of second-order accuracy in space and the self-adjoint term is discretized with symmetrical fluxes.

Remark 3.1. Though the generalized Slotboom reformulation transforms the convective term and diffusive term into a self-adjoint elliptic operator, abandoning the benefit of constant-coefficient Laplacian discretizations, this treatment can lead to the unconditional MBP-preserving schemes with second-order convergence in space. This result not only can release the restriction of the time step and generate less discrete linear systems for a fixed simulation time, but also can achieve similar computational accuracy with a much larger mesh (which means much smaller discrete linear system) comparing with the first-order schemes. Moreover, in the practical implementation, the variable-coefficient system generated by the reformulation can be solved efficiently by the classical generalized minimal residual (GMRES) methods due to its positivity.

It should be noted that the stabilizing term in the above will lead to the explicit treatment of the nonlinear term $f_\kappa^\epsilon(u)$ while avoiding a strict time step constraint. And the stabilizing parameter κ in (3.4) is always well-defined since the nonlinear function $f(u)$ is continuously differentiable. Moreover, we have the following lemma regarding the nonlinear function term.

Lemma 3.1 ([13])**.** *Suppose that Assumption* 2.1 *and the requirement* (3.4) *are satisfied, then there hold, for any* $\xi,\eta\in[-\beta,\beta]$,

(i) $\left|f_\kappa^\epsilon(\xi)\right|\le\dfrac{\kappa}{\epsilon^2}\beta$,

(ii) $\left|f_\kappa^\epsilon(\xi)-f_\kappa^\epsilon(\eta)\right|\le\dfrac{2\kappa}{\epsilon^2}|\xi-\eta|$.

3.1 Discrete maximum bound principle

We have the following theorem on the MPB for the SI scheme (3.7).

Theorem 3.1 (Unconditional Discrete MBP of the SI Scheme)**.** *Suppose that Assumption* 2.1 *and the requirement* (3.4) *are satisfied. Given* $u^n\in\mathcal{C}$ *with* $\|u^n\|_\infty\le\beta$, *then there exists a unique solution* $u^{n+1}\in\mathcal{C}$ *to the SI scheme* (3.7) *with* $\|u^{n+1}\|_\infty\le\beta$ *for any time step size* $\tau>0$.

Proof. It suffices to prove $\|u^{n+1}\|_\infty\le\beta$ if $\|u^n\|_\infty\le\beta$. Under the periodic boundary condition, the fully discrete scheme (3.7) with the numerical flux (3.6) can be expressed in a matrix form

$$A_1u^{n+1}=u^n+\tau f_\kappa^\epsilon(u^n), \tag{3.9}$$

where $A_1=((1+\kappa\tau/\epsilon^2)I-\tau B)$ with B being the coefficient matrix resulting from the numerical discretization operator $\widetilde{\mathcal{Q}}_h^{n+1}$ related to the velocity variable $\mathbf{v}^{n+1}$.

Next, we will prove that A_1 is an M-matrix. Following the idea in [3, 11], we go through the nonzero entries in each column of matrix B. Defining

$$[i,j]=(i-1)N+j, \quad i,j=1,2,\ldots,N,$$

and then non-zero entries of the q-th column ($q=[i,j]$) are given by

$$B_{p,q}=\frac{2}{h^2}\begin{cases} \dfrac{1}{1+e^{h(v_1^{n+1})_{i-1/2,j}}}, & p=[\mathrm{mod}(i-1,N),j],\\ \dfrac{1}{1+e^{h(v_2^{n+1})_{i,j-1/2}}}, & p=[i,\mathrm{mod}(j-1,N)],\\ -\dfrac{1}{1+e^{-h(v_1^{n+1})_{i+1/2,j}}}-\dfrac{1}{1+e^{-h(v_2^{n+1})_{i,j+1/2}}} & \\ \quad -\dfrac{1}{1+e^{h(v_2^{n+1})_{i,j-1/2}}}-\dfrac{1}{1+e^{h(v_1^{n+1})_{i-1/2,j}}}, & p=q,\\ \dfrac{1}{1+e^{-h(v_2^{n+1})_{i,j+1/2}}}, & p=[i,\mathrm{mod}(j+1,N)],\\ \dfrac{1}{1+e^{-h(v_1^{n+1})_{i+1/2,j}}}, & p=[\mathrm{mod}(i+1,N),j], \end{cases}$$

where $\mathrm{mod}(k,l)$ returns the remainder of k divided by l. Furthermore, we observe the following property:

$$\begin{cases} \sum\limits_{p=1}^{N^2} B_{p,q}=0, & q=1,2,\ldots,N^2,\\ B_{q,q}<0, & q=1,2,\ldots,N^2,\\ B_{p,q}\geq 0, & p,q=1,2,\ldots,N^2, \quad p\neq q. \end{cases}$$

Additionally, we have

$$-B_{q,q}=\sum_{p=1,p\neq q}^{N^2} B_{p,q}, \quad q=1,2,\ldots,N^2.$$

Thus, the matrix $A_1=((1+\kappa\tau/\epsilon^2)I-\tau B)$ has positive diagonal terms and nonpositive offdiagonal terms and is strictly diagonally dominant with respect to its columns. This means that A is an M-matrix and thus invertible and its inverse has only nonnegative coefficients.

To prove $u_{i,j}^{n+1}\leq\beta$ for any $(x_i,y_j)\in\bar{\Omega}$, we rewrite (3.9) as

$$A_1(u^{n+1}-\beta)=(u^n-\beta)+\tau\left(f_\kappa^\epsilon(u^n)-\frac{\kappa}{\epsilon^2}\beta\right).$$

According to Lemma 2.1, using $u_{i,j}^n\leq\beta$ yields

$$(u^n-\beta)+\tau\left(f_\kappa^\epsilon(u^n)-\frac{\kappa}{\epsilon^2}\beta\right)\leq 0,$$

which implies that

$$A_1(u^{n+1}-\beta)\leq 0.$$

As A_1 is an M-matrix, we conclude that $u_{i,j}^{n+1}\leq\beta$. We can prove in exactly the same way that, for any $(x_i,y_j)\in\bar{\Omega}$,

$$A_1(u^{n+1}+\beta)=(u^n+\beta)+\tau\left(f_\kappa^\epsilon(u^n)+\frac{\kappa}{\epsilon^2}\beta\right)\geq 0,$$

which gives $u_{i,j}^{n+1}\geq-\beta$. Thus, we obtain that $\|u^{n+1}\|_\infty\leq\beta$. The proof is complete. □

Remark 3.2. According to the requirement (3.4) on the stabilizing parameter for the SI scheme (3.7), with simple calculations, we can choose $\kappa=2$ for the double well potential (2.3) with the bounding constant $\beta=1$, and $\kappa\approx 8.02$ for the Flory-Huggins potential (2.4) with $\theta=0.8$ and $\theta_c=1.6$ and the bounding constant $\beta\approx 0.9575$ [13].

3.2 Convergence analysis

Below we will derive error estimate for the SI scheme (3.7). It is worth noting that c and c_i $(i\in\mathbb{Z})$ used in the following are generic positive constants independent of h and τ. Define $U^n:=\mathcal{I}_h u(x,y,t_n)$ as the corresponding grid functions in the spatial mesh at time t_n. Then, the model equation (2.7) can be rewritten as

$$\frac{U^{n+1}-U^n}{\tau}=\widetilde{\mathcal{Q}}_h^{n+1}U^{n+1}-\frac{\kappa}{\epsilon^2}U^{n+1}+f_\kappa^\epsilon(U^n)+R^{n+1} \tag{3.10}$$

with the truncation error given by

$$\begin{aligned}R^{n+1}=&\frac{U^{n+1}-U^n}{\tau}-U_t^{n+1}+f_\kappa^\epsilon(U^{n+1})-f_\kappa^\epsilon(U^n)\\&+\left(e^{w_1^{n+1}}\left(e^{-w_1^{n+1}}U^{n+1}\right)_x\right)_x+\left(e^{w_2^{n+1}}\left(e^{-w_2^{n+1}}U^{n+1}\right)_y\right)_y-\widetilde{\mathcal{Q}}_h^{n+1}U^{n+1},\end{aligned} \tag{3.11}$$

where $w_1^{n+1}:=w_1(x,y,t_{n+1})$ and $w_2^{n+1}:=w_2(x,y,t_{n+1})$.

Lemma 3.2. *Suppose that Assumption* 2.1 *and the requirement* (3.4) *are satisfied. Assume that the solution to the model equation* (2.7) *belongs to* $C^2(0,T;C(\Omega))\cap C(0,T;C^4(\Omega))$ *and* $\mathbf{v}\in C(0,T;C^3(\Omega)^2)$. *Then, the following estimate holds:*

$$\|R^{n+1}\|_\infty\leq c_1(\tau+h^2). \tag{3.12}$$

Proof. For the first four terms in R^{n+1} defined in (3.11), using the identity transformation with respect to the time derivative approximation and Lemma 3.1 respectively, we have

$$\begin{aligned}\left\|\frac{U^{n+1}-U^n}{\tau}-U_t^{n+1}\right\|_\infty&=\left\|\mathcal{I}_h\left(\frac{u(t_{n+1})-u(t_n)}{\tau}-u_t(t_{n+1})\right)\right\|_\infty\\&=\left\|\frac{1}{\tau}\int_{t_n}^{t_{n+1}}(s-t_n)\mathcal{I}_h u_{tt}(s)\mathrm{d}s\right\|_\infty\\&\leq c\tau\|u\|_{C^2(0,T;C(\Omega))},\end{aligned} \tag{3.13}$$

and

$$\left\|f_\kappa^\epsilon(U^{n+1})-f_\kappa^\epsilon(U^n)\right\|_\infty \le \frac{2\kappa}{\epsilon^2}\left\|\mathcal{I}_h\big(u(t_{n+1})-u(t_n)\big)\right\|_\infty \le c\frac{2\kappa\tau}{\epsilon^2}\|u\|_{C^1(0,T;C(\Omega))}. \tag{3.14}$$

For the last two terms in R^{n+1}, there holds that

$$\begin{aligned}
&\left\|\left(e^{w_1^{n+1}}\left(e^{-w_1^{n+1}}U^{n+1}\right)_x\right)_x+\left(e^{w_2^{n+1}}\left(e^{-w_2^{n+1}}U^{n+1}\right)_y\right)_y-\widetilde{\mathcal{Q}}_hU^{n+1}\right\|_\infty\\
\le&\left\|\left(e^{w_1^{n+1}}\left(e^{-w_1^{n+1}}U^{n+1}\right)_x\right)_x+\left(e^{w_2^{n+1}}\left(e^{-w_2^{n+1}}U^{n+1}\right)_y\right)_y\right.\\
&\quad -d_x\left(e^{w_1^{n+1}}d_x\left(e^{-w_1^{n+1}}U^{n+1}\right)\right)-d_y\left(e^{w_2^{n+1}}d_y\left(e^{-w_2^{n+1}}U^{n+1}\right)\right)\Big\|_\infty\\
&\quad +\left\|d_x\left(e^{w_1^{n+1}}d_x\left(e^{-w_1^{n+1}}U^{n+1}\right)\right)+d_y\left(e^{w_2^{n+1}}d_y\left(e^{-w_2^{n+1}}U^{n+1}\right)\right)-\mathcal{Q}_h^{n+1}U^{n+1}\right\|_\infty\\
&\quad +\left\|\mathcal{Q}_h^{n+1}U^{n+1}-\widetilde{\mathcal{Q}}_h^{n+1}U^{n+1}\right\|_\infty\\
=&\,I_1+I_2+I_3.
\end{aligned}\tag{3.15}$$

Noting the definitions of the discrete gradient and Laplacian operators, we have

$$\begin{aligned}
I_1=&\left\|\left(e^{w_1^{n+1}}\left(e^{-w_1^{n+1}}U^{n+1}\right)_x\right)_x+\left(e^{w_2^{n+1}}\left(e^{-w_2^{n+1}}U^{n+1}\right)_y\right)_y\right.\\
&\quad -d_x\left(e^{w_1^{n+1}}d_x\left(e^{-w_1^{n+1}}U^{n+1}\right)\right)-d_y\left(e^{w_2^{n+1}}d_y\left(e^{-w_2^{n+1}}U^{n+1}\right)\right)\Big\|_\infty\\
\le&\left\|\left(e^{w_1^{n+1}}\left(e^{-w_1^{n+1}}U^{n+1}\right)_x\right)_x-d_x\left(e^{w_1^{n+1}}d_x\left(e^{-w_1^{n+1}}U^{n+1}\right)\right)\right\|_\infty\\
&\quad +\left\|\left(e^{w_2^{n+1}}\left(e^{-w_2^{n+1}}U^{n+1}\right)_y\right)_y-d_y\left(e^{w_2^{n+1}}d_y\left(e^{-w_2^{n+1}}U^{n+1}\right)\right)\right\|_\infty\\
=&\left\|(\partial_x-d_x)\left(e^{w_1^{n+1}}\left(e^{-w_1^{n+1}}U^{n+1}\right)_x\right)+d_x\left(e^{w_1^{n+1}}(\partial_x-d_x)\left(e^{-w_1^{n+1}}U^{n+1}\right)\right)\right\|_\infty\\
&\quad +\left\|(\partial_y-d_y)\left(e^{w_2^{n+1}}\left(e^{-w_2^{n+1}}U\right)_y\right)+d_y\left(e^{w_2^{n+1}}(\partial_y-d_y)\left(e^{-w_2^{n+1}}U\right)\right)\right\|_\infty\\
\le&\,\mathrm{ch}^2\|\mathbf{v}\|^2_{C(0,T;C^3(\Omega))}\|u\|_{C(0,T;C^4(\Omega))}.
\end{aligned}$$

It follows from the harmonic mean approximation for the half point value that

$$\begin{aligned}
I_2=&\left\|d_x\left(e^{w_1^{n+1}}d_x\left(e^{-w_1^{n+1}}U^{n+1}\right)\right)+d_y\left(e^{w_2^{n+1}}d_y\left(e^{-w_2^{n+1}}U^{n+1}\right)\right)-\mathcal{Q}_h^{n+1}U^{n+1}\right\|_\infty\\
\le&\left\|d_x\left(e^{w_1^{n+1}}d_x\left(e^{-w_1^{n+1}}U^{n+1}\right)\right)-d_x\left(\overline{e^{w_1^{n+1}}}d_x\left(e^{-w_1^{n+1}}U^{n+1}\right)\right)\right\|_\infty\\
&\quad +\left\|d_y\left(e^{w_2^{n+1}}d_y\left(e^{-w_2^{n+1}}U^{n+1}\right)\right)-d_y\left(\overline{e^{w_2^{n+1}}}d_y\left(e^{-w_2^{n+1}}U^{n+1}\right)\right)\right\|_\infty\\
=&\left\|d_x\left(\left(e^{w_1^{n+1}}-\overline{e^{w_1^{n+1}}}\right)d_x\left(e^{-w_1^{n+1}}U^{n+1}\right)\right)\right\|_\infty+\left\|d_y\left(\left(e^{w_2^{n+1}}-\overline{e^{w_2^{n+1}}}\right)d_y\left(e^{-w_2^{n+1}}U^{n+1}\right)\right)\right\|_\infty\\
\le&\,\mathrm{ch}^2\|\mathbf{v}\|^2_{C(0,T;C^3(\Omega))}\|u\|_{C(0,T;C^4(\Omega))}.
\end{aligned}$$

According to the midpoint formula, we get

$$I_3=\left\|\mathcal{Q}_h^{n+1}U^{n+1}-\widetilde{\mathcal{Q}}_h^{n+1}U^{n+1}\right\|_\infty \le \mathrm{ch}^2\|\mathbf{v}\|^2_{C(0,T;C^3(\Omega))}\|u\|_{C(0,T;C^4(\Omega))}. \tag{3.16}$$

Putting the above inequalities into (3.15), and combining (3.11) with (3.13)-(3.15), we obtain the desired result. □

Lemma 3.3. *Under the assumption of Lemma* 3.2*, for the nonlinear diffusion operator defined in* (3.8)*, there holds that for any* $h\in(0,1]$*,*

$$\left\langle \widetilde{\mathcal{Q}}_h^{n+1}u^{n+1},u^{n+1}\right\rangle_h \leq -\frac{1}{2}\left\|\nabla_h u^{n+1}\right\|_h^2+c_2\|u^{n+1}\|_h^2.$$

Proof. First, it follows from (2.8) that

$$\begin{aligned}&\left\langle \mathcal{Q}_h^{n+1}u^{n+1},u^{n+1}\right\rangle_h\\ =&-\left\langle \overline{e^{w_1^{n+1}}}d_x\left(e^{-w_1^{n+1}}u^{n+1}\right),d_xu^{n+1}\right\rangle_h\\ &-\left\langle \overline{e^{w_2^{n+1}}}d_y\left(e^{-w_2^{n+1}}u^{n+1}\right),d_yu^{n+1}\right\rangle_h,\end{aligned}$$

where $\overline{e^{w_1^{n+1}}}$ and $\overline{e^{w_2^{n+1}}}$ are approximated by the harmonic mean approximation (3.3).

Next using the produce rule that $d_x(fg)_{i,j}=a_xf_{i,j}d_xg_{i,j}+a_xg_{i,j}d_xf_{i,j}$ as stated in [10], we get

$$d_x\left(e^{-w_1^{n+1}}u^{n+1}\right)_{i,j}=d_x\left(e^{-w_1^{n+1}}\right)_{i,j}a_xu_{i,j}^{n+1}+a_x\left(e^{-w_1^{n+1}}\right)_{i,j}d_xu_{i,j}^{n+1},$$

which implies that

$$\begin{aligned}&\left(\overline{e^{w_1^{n+1}}}\right)_{i,j}d_x\left(e^{-w_1^{n+1}}u^{n+1}\right)_{i,j}\\ =&\left(\overline{e^{w_1^{n+1}}}\right)_{i,j}\left(d_x\left(e^{-w_1^{n+1}}\right)_{i,j}a_xu_{i,j}^{n+1}+a_x\left(e^{-w_1^{n+1}}\right)_{i,j}d_xu_{i,j}^{n+1}\right)\\ =&\left(\overline{e^{w_1^{n+1}}}\right)_{i,j}d_x\left(e^{-w_1^{n+1}}\right)_{i,j}a_xu_{i,j}^{n+1}+d_xu_{i,j}^{n+1},\end{aligned}$$

where we have used the fact from (3.3) that $(\overline{e^{w_1^{n+1}}})_{i,j}a_x(e^{-w_1^{n+1}})_{i,j}=1$ in the pointwise sense. Thus, by noting the regularity on $\mathbf{v}$ from Lemma 3.2, we conclude that

$$\begin{aligned}&\left\langle \overline{e^{w_1^{n+1}}}d_x(e^{-w_1^{n+1}}u^{n+1}),d_xu^{n+1}\right\rangle_h\\ =&\left\|d_xu^{n+1}\right\|_h^2+\left\langle a_xu^{n+1}\left(d_xe^{-w_1^{n+1}}\right)\overline{e^{w_1^{n+1}}},d_xu^{n+1}\right\rangle_h\\ \geq&\left\|d_xu^{n+1}\right\|_h^2-\left\|a_xu^{n+1}\right\|_h\|d_xe^{-w_1^{n+1}}\|_\infty\left\|\overline{e^{w_1^{n+1}}}\right\|_\infty\left\|d_xu^{n+1}\right\|_h\\ \geq&\left\|d_xu^{n+1}\right\|_h^2-c\|u^{n+1}\|_h\left\|d_xu^{n+1}\right\|_h\\ \geq&\frac{1}{2}\left\|d_xu^{n+1}\right\|_h^2-c\|u^{n+1}\|_h^2.\end{aligned}$$

Similarly, we have

$$\left\langle \overline{e^{w_2^{n+1}}}d_y\left(e^{-w_2^{n+1}}u^{n+1}\right),d_yu^{n+1}\right\rangle_h\geq\frac{1}{2}\left\|d_yu^{n+1}\right\|_h^2-c\|u^{n+1}\|_h^2.$$

Combining the above two inequalities gives

$$\left\langle \mathcal{Q}_h^{n+1}u^{n+1},u^{n+1}\right\rangle_h \leq -\frac{1}{2}\left\|\nabla_h u^{n+1}\right\|_h^2+c\|u^{n+1}\|_h^2. \tag{3.17}$$

Finally, using (3.16) and (3.17), we arrive at

$$\begin{aligned}\left\langle \widetilde{\mathcal{Q}}_h^{n+1}u^{n+1},u^{n+1}\right\rangle_h &= \left\langle \mathcal{Q}_h^{n+1}u^{n+1},u^{n+1}\right\rangle_h+\left\langle \left(\widetilde{\mathcal{Q}}_h^{n+1}-\mathcal{Q}_h^{n+1}\right)u^{n+1},u^{n+1}\right\rangle_h\\ &\leq -\frac{1}{2}\left\|\nabla_h u^{n+1}\right\|_h^2+c\|u^{n+1}\|_h^2+ch^2\|u^{n+1}\|_h^2\\ &\leq -\frac{1}{2}\left\|\nabla_h u^{n+1}\right\|_h^2+c\|u^{n+1}\|_h^2,\end{aligned}$$

where we have used $h\leq 1$. The proof is complete. □

Setting $e^n=U^n-u^n$, we can easily verify that $e^0=0$. Then, there holds the following error estimate the SI scheme (3.7).

Theorem 3.2 (Error Estimate of the SI Scheme)**.** *Under the assumptions of Lemma* 3.2*, for the numerical solutions $u^{n+1}\in\mathcal{C}$ generated by the SI scheme* (3.7)*, we have the following error estimate that, for $n=0,1,\ldots,M-1$,*

$$\|e^{n+1}\|_h+\left(\tau\sum_{k=1}^{n}\left\|\nabla_h e^{k+1}\right\|_h^2\right)^{\frac{1}{2}}\leq c(\tau+h^2).$$

Proof. Subtracting (3.7) from (3.10), we obtain

$$\frac{e^{n+1}-e^n}{\tau}+\frac{\kappa}{\epsilon^2}e^{n+1}=\widetilde{\mathcal{Q}}_h e^{n+1}+f_\kappa^\epsilon(U^n)-f_\kappa^\epsilon(u^n)+R^{n+1}. \tag{3.18}$$

Then taking the discrete inner product with e^{n+1} on both sides of (3.18), we have

$$\begin{aligned}&\frac{1}{2\tau}\left(\|e^{n+1}\|_h^2-\|e^n\|_h^2+\|e^{n+1}-e^n\|_h^2\right)+\frac{\kappa}{\epsilon^2}\|e^{n+1}\|_h^2\\ &=\left\langle \widetilde{\mathcal{Q}}_h e^{n+1},e^{n+1}\right\rangle_h+\left\langle f_\kappa^\epsilon(U^n)-f_\kappa^\epsilon(u^n),e^{n+1}\right\rangle_h+\left\langle R^{n+1},e^{n+1}\right\rangle_h.\end{aligned} \tag{3.19}$$

Next, we estimate the terms on the right-hand side of (3.19). According to Lemma 3.3, we have

$$\left\langle \widetilde{\mathcal{Q}}_h e^{n+1},e^{n+1}\right\rangle_h\leq -\frac{1}{2}\left\|\nabla_h e^{n+1}\right\|_h^2+c_2\|e^{n+1}\|_h^2.$$

Due to (3.12), the truncation error term can be bounded by

$$\left\langle R^{n+1},e^{n+1}\right\rangle_h\leq\|R^{n+1}\|_h\|e^{n+1}\|_h\leq\|e^{n+1}\|_h^2+c(\tau^2+h^4).$$

Using $\|U^n\|_\infty\leq\beta,\|u^n\|_\infty\leq\beta$ and Lemma 3.1, we get that

$$\left\|f_\kappa^\epsilon(U^n)-f_\kappa^\epsilon(u^n)\right\|_h\leq\frac{2\kappa}{\epsilon^2}\|U^n-u^n\|_h=\frac{2\kappa}{\epsilon^2}\|e^n\|_h,$$

which in turn implies that

$$\left\langle f_\kappa^\epsilon(U^n)-f_\kappa^\epsilon(u^n),e^{n+1}\right\rangle_h \le \frac{2\kappa}{\epsilon^2}\|e^n\|_h\|e^{n+1}\|_h \le \frac{\kappa}{\epsilon^2}\|e^{n+1}\|_h^2+\frac{\kappa}{\epsilon^2}\|e^n\|_h^2.$$

Putting the above inequalities into (3.19), we get

$$\|e^{n+1}\|_h^2-\|e^n\|_h^2+\tau\left\|\nabla_h e^{n+1}\right\|_h^2 \le 2(c_2+1)\tau\|e^{n+1}\|_h^2+\frac{2\kappa\tau}{\epsilon^2}\|e^n\|_h^2+c(\tau^2+h^4).$$

Taking a summation with respect to n in the above inequality and applying the discrete Gronwall lemma [21, 43], we arrive at

$$\|e^{n+1}\|_h^2+\tau\sum_{k=1}^{n}\left\|\nabla_h e^{k+1}\right\|_h^2 \le c(\tau^2+h^4).$$

The proof is complete. □

Remark 3.3. The convective Allen-Cahn equation contains a velocity vector with the divergence-free property, thus it can couple with the incompressible fluid motion, such as (Navier-)Stokes equations [37, 41, 45, 52] and Hele-Shaw equations [5, 7, 40]. The generalized Slotboom reformulation mainly focuses on the convective Allen-Cahn sub-equation in these coupled systems, thus it is very straightforward to be extended and the convergence analysis presented here can be also theoretically justified in a similar way. But there are still some technique problems when applying the idea to the convective Cahn-Hilliard equations [6, 9, 18–20] because of the complexity of the diffusion term in these models.

4 The second-order numerical scheme in both time and space

Inspired by the SI scheme (3.7), we propose the following second-order scheme for (2.7) (denoted as the SII scheme) as follows: Given $u^0=\mathcal{I}_h u_0(\mathbf{x})\in\mathcal{C}$, for $n=1,\dots,M-1$, find $u^{n+1}\in\mathcal{C}$ such that

$$\begin{aligned}\frac{u^{n+1}-u^n}{\tau}=&\frac{1}{2}\widetilde{\mathcal{Q}}_h^{n+1}u^{n+1}+\frac{1}{2}\left(\Delta_h u^n-\mathbf{v}^n\cdot\widetilde{\nabla}_h u^n\right)\\&+\frac{3}{2}f^\epsilon(u^n)-\frac{1}{2}f^\epsilon(u^{n-1})+\frac{\gamma}{\epsilon^2}(u^{n+1}-2u^n+u^{n-1})\end{aligned}\tag{4.1}$$

with $\widetilde{\nabla}_h u_{i,j}=(d_x(a_x u)_{i,j},d_y(a_y u)_{i,j})^\top$ and $\gamma>0$ is a stabilizing parameter, where the numerical fluxes are defined in (3.6). For the first step, we use the SI scheme (3.7) to find u^1.

To establish the MBP preservation of SII scheme (4.1), we shall share the following assumption regarding the nonlinear function f.

Assumption 4.1 ([25]). If there exists a constant $\beta>0$ such that $f(\pm\beta)=0$ and f is continuously differentiable and nonconstant on $[-\beta,\beta]$, then it holds that for any $\xi\in[-\beta,\beta]$,

$$\begin{aligned}&\exists\tau_0^+>0 \quad \text{such that} \quad |\xi+\tau f(\xi)|\le\beta, \quad \forall\tau\in(0,\tau_0^+],\\ &\exists\tau_0^->0 \quad \text{such that} \quad |\xi-\tau f(\xi)|\le\beta, \quad \forall\tau\in(0,\tau_0^-].\end{aligned}$$

Furthermore, we have

$$\tau_0^+=-\frac{1}{\min_{|\xi|\le\beta}f'(\xi)}, \quad \tau_0^-=\frac{1}{\max_{|\xi|\le\beta}f'(\xi)}.$$

Theorem 4.1 (Discrete MBP of the SII Scheme). *Suppose that Assumption* 4.1 *is satisfied. Given $u^k\in\mathcal{C}$ with $\|u^k\|_\infty\le\beta$, $k=n,n-1$, there exists a unique solution $u^{n+1}\in\mathcal{C}$ to the SII scheme* (4.1) *with $\|u^{n+1}\|_\infty\le\beta$ provided that $\gamma\ge1/(2\tau_0^-)$ and*

$$\tau\le\min\left(\frac{h^2}{4},\frac{\epsilon^2}{4\gamma},\frac{\epsilon^2\tau_0^+}{3+4\gamma\tau_0^+}\right), \quad h\le\frac{2}{\|\mathbf{v}\|_\infty}. \tag{4.2}$$

Proof. Under the periodic boundary condition, the fully discrete scheme (4.1) with the numerical fluxes (3.6) can be expressed in a matrix form

$$A_2u^{n+1}=\frac{1}{2}u^n+\frac{\tau}{2}Hu^n+\left(\frac{1}{2}-\frac{2\gamma\tau}{\epsilon^2}\right)u^n+\frac{3\tau}{2}f^\epsilon(u^n)+\frac{\gamma\tau}{\epsilon^2}u^{n-1}-\frac{\tau}{2}f^\epsilon(u^{n-1}), \tag{4.3}$$

where

$$A_2=\left(\left(1-\frac{\gamma\tau}{\epsilon^2}\right)I-\frac{\tau}{2}B\right)$$

and H is a coefficient matrix resulting from numerical discretization $\Delta_h-\mathbf{v}^n\cdot\widetilde{\nabla}_h$. Following the same proof in Theorem 3.1, if $\tau\le\epsilon^2/\gamma$, then A_2 is an M-matrix.

To prove $u_{i,j}^{n+1}\le\beta$ for any $(x_i,y_j)\in\bar{\Omega}$, we rewrite (4.3) as

$$\begin{aligned}A_2(u^{n+1}-\beta)&=\frac{1}{2}u^n+\frac{\tau}{2}Hu^n+\left(\frac{1}{2}-\frac{2\gamma\tau}{\epsilon^2}\right)u^n+\frac{3\tau}{2}f^\epsilon(u^n)\\&\quad+\frac{\gamma\tau}{\epsilon^2}u^{n-1}-\frac{\tau}{2}f^\epsilon(u^{n-1})-\left(1-\frac{\gamma\tau}{\epsilon^2}\right)\beta\\&=K_1+K_2+K_3-\left(1-\frac{\gamma\tau}{\epsilon^2}\right)\beta.\end{aligned} \tag{4.4}$$

From the definitions of $\widetilde{\nabla}_h$ and Δ_h, we have that $\|I+\tau H\|_\infty\le1$ if $\tau\le h^2/4$ and $h\le2/\|\mathbf{v}\|_\infty$, which yields that

$$\|K_1\|_\infty=\frac{1}{2}\|(I+\tau H)u^n\|_\infty\le\frac{1}{2}\|I+\tau H\|_\infty\|u^n\|_\infty\le\frac{\beta}{2}. \tag{4.5}$$

According to Assumption 4.1, we derive that if

$$\tau\le\min\left(\frac{\epsilon^2}{4\gamma},\frac{\epsilon^2\tau_0^+}{3+4\gamma\tau_0^+}\right),$$

then

$$\begin{aligned}\|K_2\|_\infty &= \left\| \left(\frac{1}{2}-\frac{2\gamma\tau}{\epsilon^2}\right)u^n+\frac{3\tau}{2}f^\epsilon(u^n)\right\|_\infty \\ &\le \left(\frac{1}{2}-\frac{2\gamma\tau}{\epsilon^2}\right)\left\|u^n+\frac{3\tau}{\epsilon^2-4\gamma\tau}f(u^n)\right\|_\infty \le \left(\frac{1}{2}-\frac{2\gamma\tau}{\epsilon^2}\right)\beta. \end{aligned} \tag{4.6}$$

Similarly, if $\gamma \ge 1/(2\tau_0^-)$, then

$$\|K_3\|_\infty = \left\|\frac{\gamma\tau}{\epsilon^2}u^{n-1}-\frac{\tau}{2}f^\epsilon(u^{n-1})\right\|_\infty \le \frac{\gamma\tau}{\epsilon^2}\left\|u^{n-1}-\frac{1}{2\gamma}f(u^{n-1})\right\|_\infty \le \frac{\gamma\tau}{\epsilon^2}\beta. \tag{4.7}$$

Putting (4.5)-(4.7) into (4.4) gives

$$A_2(u^{n+1}-\beta) = K_1+K_2+K_3-\left(1-\frac{\gamma\tau}{\epsilon^2}\right)\beta \le 0,$$

which implies $u_{i,j}^{n+1} \le \beta$ by noting that A_2 is an M-matrix. $u_{i,j}^{n+1} \ge -\beta$ can be obtained in a similar way. Thus, we obtain $\|u^{n+1}\|_\infty \le \beta$. The proof is complete. □

Remark 4.1. According to Assumption 4.1, $\tau_0^+ = 1/2$ and $\tau_0^- = 1$ is deduced for the double well potential (2.3) with the bounding constant

$$\beta = 1, \quad \tau_0^+ = \frac{1-\beta^2}{\theta-\theta_c(1-\beta^2)} \approx 0.1248, \quad \tau_0^- = \frac{1}{\theta_c-\theta} = \frac{5}{4}$$

is deduced for the Flory-Huggins potential (2.4) with $\theta = 0.8$ and $\theta_c = 1.6$ and the bounding constant $\beta \approx 0.9575$ [25]. Under the requirement on the stabilizing parameter from Theorem 4.1, we can choose $\gamma = 1/2$ consistently for the double well potential (2.3) and the Flory-Huggins potential (2.4) with $\theta = 0.8$ and $\theta_c = 1.6$.

Remark 4.2. It is worth noting that an alternative second-order scheme (denoted as the SII-CN scheme) can be proposed as follows:

$$\begin{aligned}\frac{u^{n+1}-u^n}{\tau} &= \frac{1}{2}\widetilde{\mathcal{Q}}_h^{n+1}u^{n+1}+\frac{1}{2}\widetilde{\mathcal{Q}}_h^n u^n+\frac{3}{2}f^\epsilon(u^n) \\ &\quad -\frac{1}{2}f^\epsilon(u^{n-1})+\frac{\gamma}{\epsilon^2}(u^{n+1}-2u^n+u^{n-1}),\end{aligned} \tag{4.8}$$

where the numerical fluxes are defined in (3.6). However, since the row sums of coefficient matrix resulting from $\widetilde{\mathcal{Q}}_h$ are not guaranteed to be non-positive, it is difficult to theoretically establish the discrete MBP for the SII-CN scheme (4.8).

Remark 4.3. In Theorem 4.1, the restriction (4.2) is needed for the second-order scheme in time. But this is a sufficient but may be not necessary condition. The reason is that, compared with other explicit schemes with the same convergence order and restriction

between the time step and the mesh size (such as the explicit Runge-Kutta scheme [23]), our simulations imply that the second-order scheme considered here have more relaxable restriction on the time step. However, how to improve this assumption is still a challenging problem, which will be considered in future.

Remark 4.4. Though we only present the convergence result for the first-order scheme, the error estimates can be generalized to the second-order cases by using the discrete MBP-preserving properties. As in the proof of Theorem 3.2, only Lemma 3.3 and the maximum bounds of the numerical solutions are used essentially, thus these results also hold for the second-order schemes.

5 Numerical experiments

In this section, we will perform some examples to numerically verify the theoretical results and demonstrate the performance of the proposed schemes. It should be noted that the periodic boundary condition is always imposed and the computational domain is set to be $\Omega=(0,1)^2$ in two dimensions and $\Omega=(0,1)^3$ in three dimensions, respectively. All computations are performed using MATLABR2022a on a Surface Pro 9 with 12th Gen Intel(R) Core(TM) i5-1235U 2.50GHz processors and 8GB of RAM.

5.1 Convergence test

In this subsection, we test the convergence order of the proposed scheme. The nonlinear function is chosen as the double well potential (2.3). The interface parameter is set as $\epsilon=0.1$ and the terminal time $T=0.01$. Given the initial value

$$u_0(x,y)=\cos(2\pi x)\cos(2\pi y)$$

and the velocity field

$$\mathbf{v}(x,y,t)=e^{-t}[\sin(2\pi y),\sin(2\pi x)]^\top$$

satisfying the divergence-free condition, we begin by testing the temporal convergence order by fixing the spatial mesh size $h=1/128$. Since there is no exact solution available, we treat the solution produced by the SII scheme with $\tau=T/1024$ as the reference solution. The temporal errors and the corresponding convergence rates with the successive time step sizes of the SI, SII and SII-CN schemes are reported in Table 1, where the expected temporal convergence accuracies are clearly observed (1 for the SI scheme and 2 for the SII and SII-CN schemes). Additionally, the SII scheme exhibits almost the same error results as the SII-CN scheme. We also compare the numerical performance with the explicit TVD-RK2 scheme [23]. For the fixed mesh size $h=1/128$, only the numerical solutions produced by TVD-RK2 schemes with $\tau=T/1024$ are available, other numerical

Table 1: The temporal errors with the corresponding convergence rates of the SI, SII and SII-CN schemes.

	T/τ	$\|\cdot\|_\infty$	Rate	$\|\cdot\|_h$	Rate
SI scheme	64	2.8264e-03	–	1.7553e-03	–
	128	1.3346e-03	1.08	8.2976e-04	1.08
	256	5.7542e-04	1.21	3.5794e-04	1.21
	512	1.9238e-04	1.58	1.1970e-04	1.58
SII scheme	64	7.9880e-05	–	4.2439e-05	–
	128	1.9923e-05	2.00	1.0595e-05	2.00
	256	4.7654e-06	2.06	2.5352e-06	2.06
	512	9.5517e-07	2.32	5.0821e-07	2.32
SII-CN scheme	64	7.9880e-05	–	4.2439e-05	–
	128	1.9923e-05	2.00	1.0595e-05	2.00
	256	4.7654e-06	2.06	2.5351e-06	2.06
	512	9.5517e-07	2.32	5.0821e-07	2.32

solutions with $\tau = T/2^k$ ($k = 2,3,\ldots,9$) produced by TVD-RK2 schemes blow up in a finite time. On the contrary, the SII scheme proposed in this paper can work well in all above computational environments, which implies that the SII scheme considered here has more relaxable restriction on the time step than the explicit TVD-RK2 scheme.

Next, we test the convergence order in space by fixing the time step size $\tau = T$. The solution produced by the SI scheme with $h = 1/1024$ is treated as the reference solution. The spatial errors and the corresponding convergence rates with the successive space step sizes are presented in Table 2. As we can see, the spatial convergence rates are of second-order, which is in line with the theoretical predictions. We also compare the CPU time of the traditional conjugate gradient (CG) method and the GMRES method to compute the variable-coefficient linear system with different mesh sizes h, which is listed in Table 3. It can be seen that compared with the CG method, the GMRES method requires much less computational time and can solve the variable-coefficient linear system very efficiently.

Table 2: The spatial errors with the corresponding convergence rates of the SI scheme.

$1/h$	$\|\cdot\|_\infty$	Rate	$\|\cdot\|_h$	Rate
64	1.8325e-03	–	1.1820e-03	–
128	4.7988e-04	1.93	3.1094e-04	1.93
256	1.2172e-04	1.98	7.8754e-05	1.98
512	3.0531e-05	2.00	1.9753e-05	2.00

Table 3: The CPU time to compute the variable-coefficient linear system at each time step.

$1/h$	128	256	512	1024
CG(s)	0.10	0.45	2.56	13.06
GMRES(s)	0.005	0.015	0.05	0.46

5.2 MBP test

In this subsection, we numerically simulate the MBP preservation of the proposed schemes for the convective Allen-Cahn equation. The initial guess is generated by the random uniform distribution between -0.9 and 0.9. The velocity field is set as

$$\mathbf{v}(x,y,t)=e^{-t-x}[\cos(y),\sin(y)]^{\top}$$

satisfying the divergence-free condition [28], which gradually tends to zero as time t becomes very large. The interface parameter is set as $\epsilon=0.01$.

Firstly, given the uniform spatial step size h=1/128, we start the simulation in the case of double well potential (2.3). Fig. 1 illustrates the evolutions of the supremum norm and the energy (defined in (1.1)) produced by the SI, SII and SII-CN schemes with τ=1e-4 and $\tau=$1e-5, where the green line $y=1$ gives the theoretical maximum bound. We also plot the snapshots of numerical solutions produced by these schemes at $t=0.001,0.005,0.02$, and 0.05 with $\tau=$1e-5 in Fig. 2. From these figures, we can observe that the discrete

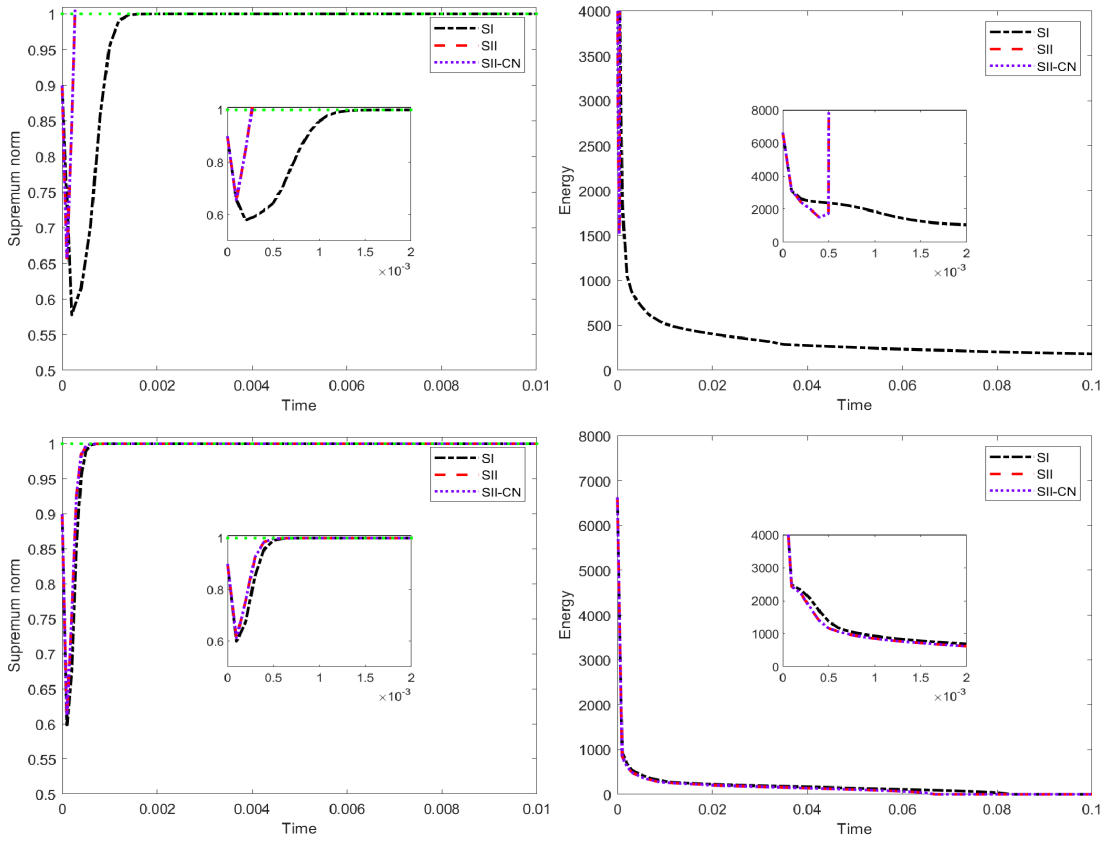

Figure 1: Evolutions of the supremum norm and the energy of the numerical solution produced by the SI, SII and SII-CN schemes for the double well potential case of the convective Allen-Cahn equation with τ=1e-4 (top) and $\tau=$1e-5 (bottom).

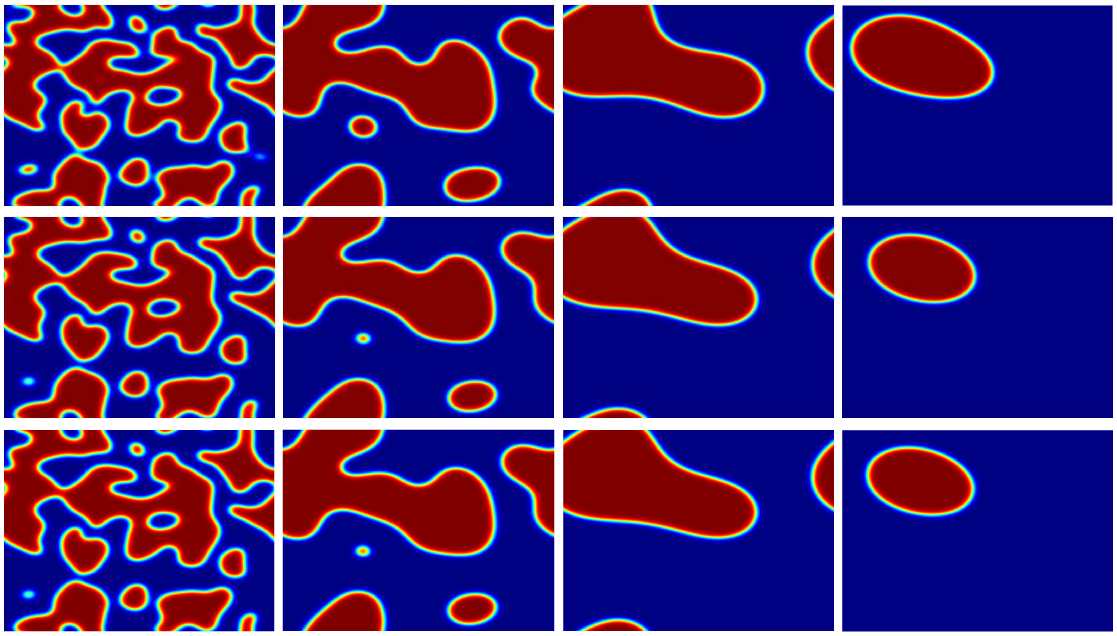

Figure 2: Numerical solutions produced by the SI (top), SII (middle) and SII-CN (bottom) schemes at $t=$ 0.001,0.005,0.02, and 0.05 (left to right) for the double well potential case of the convective Allen-Cahn equation with $\tau=$1e-5.

MBP and energy stability are preserved for all schemes with $\tau=$1e-5 and only for the SI scheme with $\tau=$1e-4. Though the energy dissipation law is not satisfied theoretically for the convective Allen-Cahn equation), which means the discrete MBP is preserved unconditionally for the SI scheme and conditionally for the SII and SII-CN schemes, which is in agreement with the theoretical results.

Secondly, with the same parameter settings as above, we consider the Flory-Huggins potential (2.4) with $\theta=0.8$ and $\theta_c=1.6$. Fig. 3 illustrates the evolutions of the supremum norm and the energy computed by the SI, SII and SII-CN schemes with $\tau=$1e-4 and $\tau=$1e-5, where the green line $y=0.9575$ gives the theoretical maximum bound. The snapshots of the numerical solutions at $t=0.001,0.005,0.02$, and 0.05 produced by these schemes with $\tau=$1e-5 are also reported in Fig. 4. From these figures, we can observe similar phenomena as in the double well potential case, which confirms the correctness and efficiency of the proposed schemes again.

5.3 Convection test

In this subsection, we will simulate the convection phenomena for the convective Allen-Cahn equation with $\epsilon=0.01$. Note that the SII scheme is used in all the following experiments. The initial value is generated by the random uniform distribution between -0.9 and 0.9. The velocity field is chosen as $\mathbf{v}(x,y,t)=500\times[y-0.5,0.5-x]^\top$, which rotates

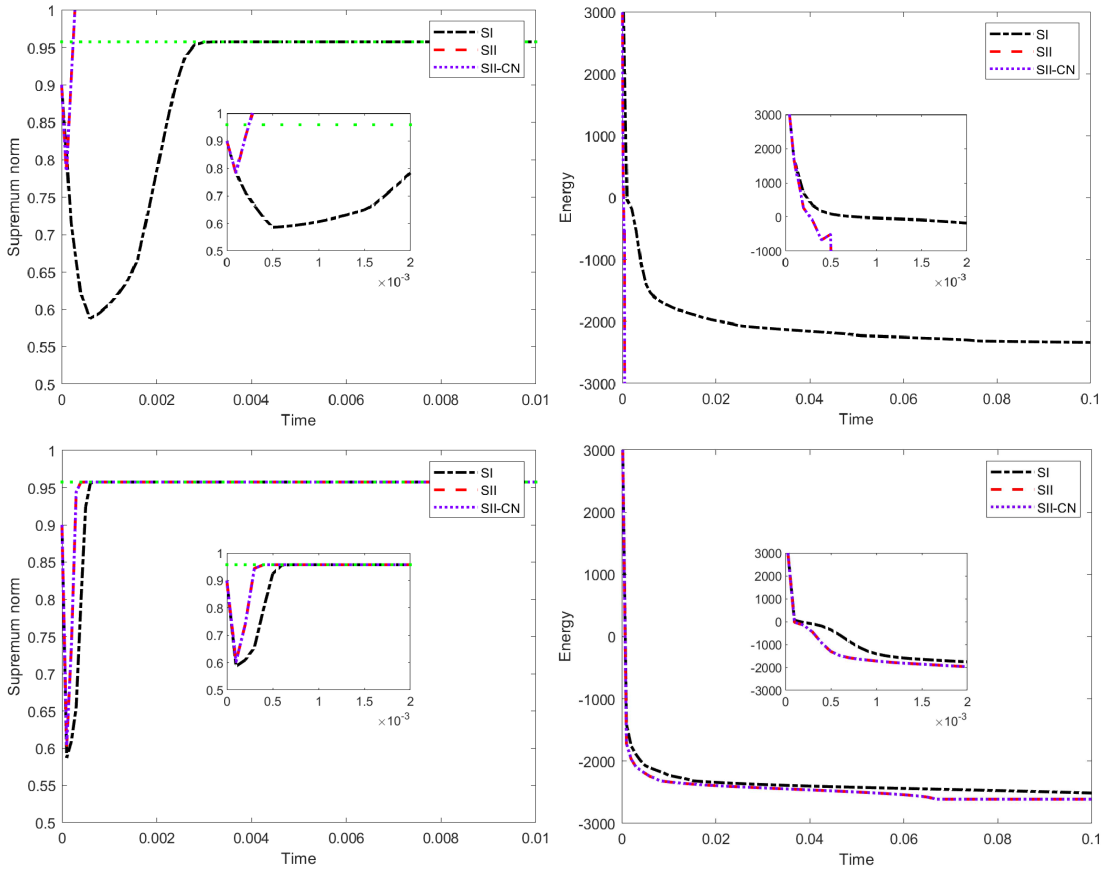

Figure 3: Evolutions of the supremum norm and the energy of the numerical solution produced by the SI, SII and SII-CN schemes for the Flory-Huggins potential case of the convective Allen-Cahn equation with $\tau=$1e-4 (top) and $\tau=$1e-5 (bottom).

clockwise around the center $(0.5,0.5)$ [44]. The time step size is chosen as $\tau=$1e-5 and the mesh size $h=1/128$.

Fig. 5 presents the snapshots of the numerical solutions at $t=0.001,0.01,0.02$ and 0.05 for the double well potential case. The corresponding evolutions of the supremum norm and the energy are illustrated in Fig. 6 where the green line $y=1$ gives the theoretical maximum bound. The discrete MBP and energy stability are indeed well preserved. Additionally, we clearly observe the ordering and coarsening phenomena as well as the rotational effect induced by the convective term along the time evolution.

We then simulate the case of Flory-Huggins potential function with θ=0.8 and θ_c=1.6. Fig. 7 depicts the configurations of the numerical solutions at $t=0.001,0.01,0.02$ and 0.05. The corresponding evolutions of the supremum norm and the energy are given in Fig. 8 where the green line $y=0.9575$ gives the theoretical maximum bound. It can be seen that the discrete MBP and the energy are well preserved again. Moreover, the rotational phenomenon is also observed as expected.

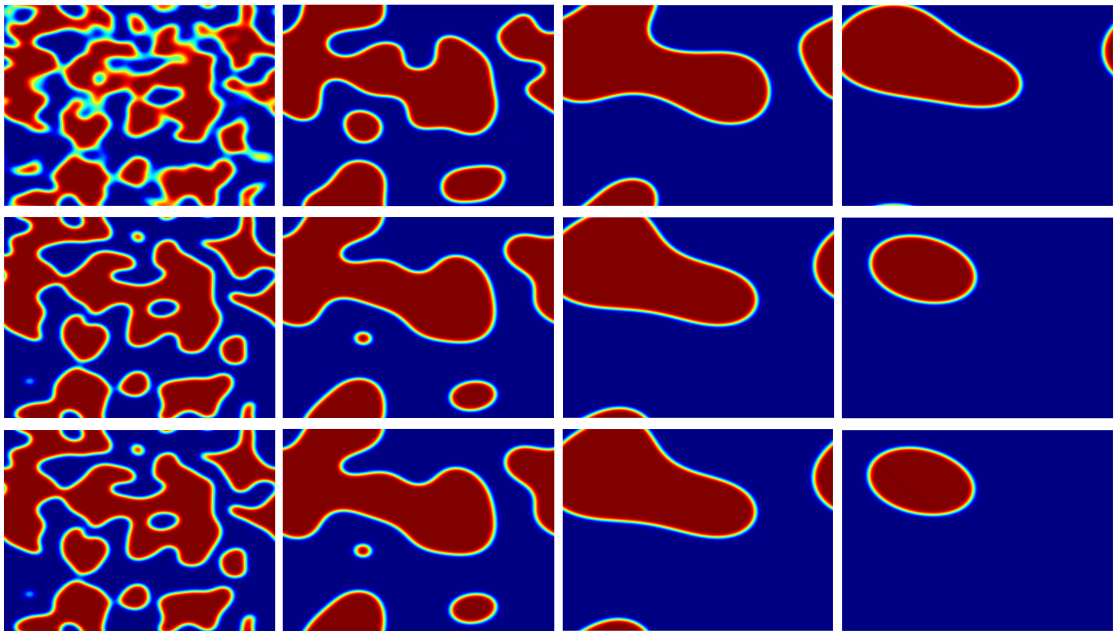

Figure 4: Numerical solutions produced by the SI (top), SII (middle) and SII-CN (bottom) schemes at $t=0.001,0.005,0.02$, and 0.05 (left to right) for the Flory-Huggins potential case of the convective Allen-Cahn equation with $\tau=$1e-5.

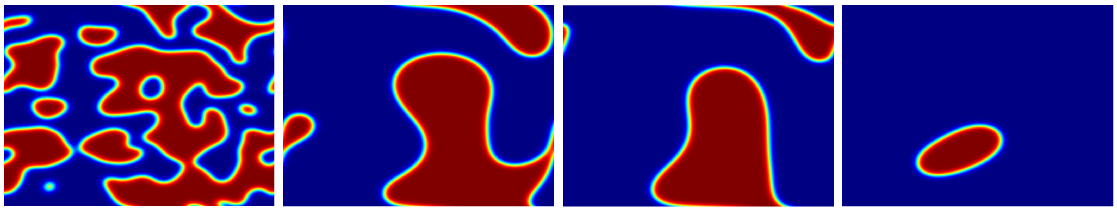

Figure 5: Numerical solutions produced by the SII scheme at $t=0.001,0.01,0.02$ and 0.05 (left to right) for the double well potential case of the convective Allen-Cahn equation.

5.4 Problems on unit circular domain

Though the schemes presented above are based on problems on tensor domains, it is very straightforward to extend this method to non-tensor domains. In this test, we consider problems with the homogeneous Dirichlet boundary condition on a unit circular domain

$$\Omega=\{(x,y)\in\mathbb{R}^2\,|\,x^2+y^2<1\}.$$

Let the initial value

$$u_0(x,y)=0.9e^{-8(x^2+y^2)}(1-x^2-y^2)^2,$$

the velocity field

$$\mathbf{v}(x,y,t)=e^{-t}[\sin(2\pi y),\sin(2\pi x)]^\top,$$

$\tau=$1e-5 and $\epsilon=0.1$. The unit circular domain is uniformly contained within the rectan-

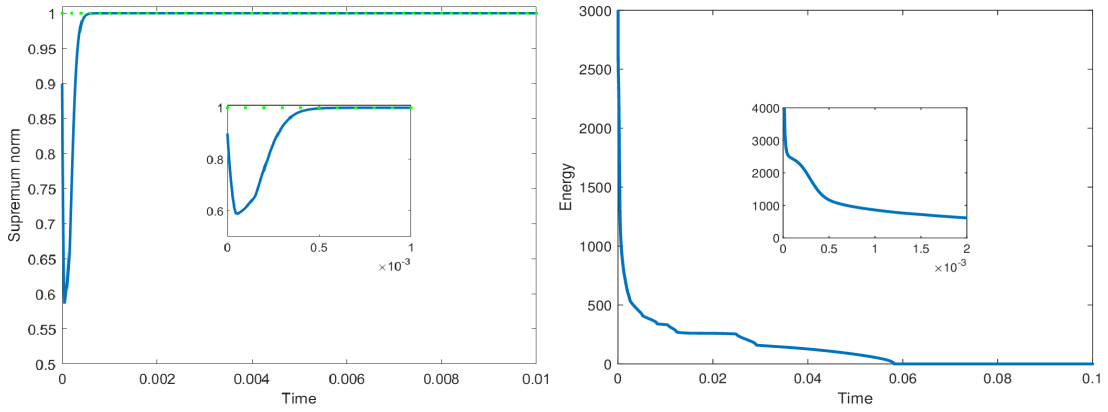

Figure 6: Evolutions of the supremum norm and the energy of numerical solution produced by the SII scheme for the double well potential case of the convective Allen-Cahn equation.

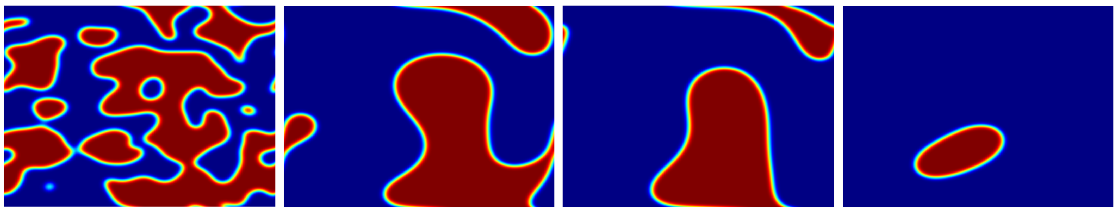

Figure 7: Numerical solutions produced by the SII scheme at $t=0.001,0.01,0.02$ and 0.05 (left to right) for the Flory-Huggins potential case of the convective Allen-Cahn equation.

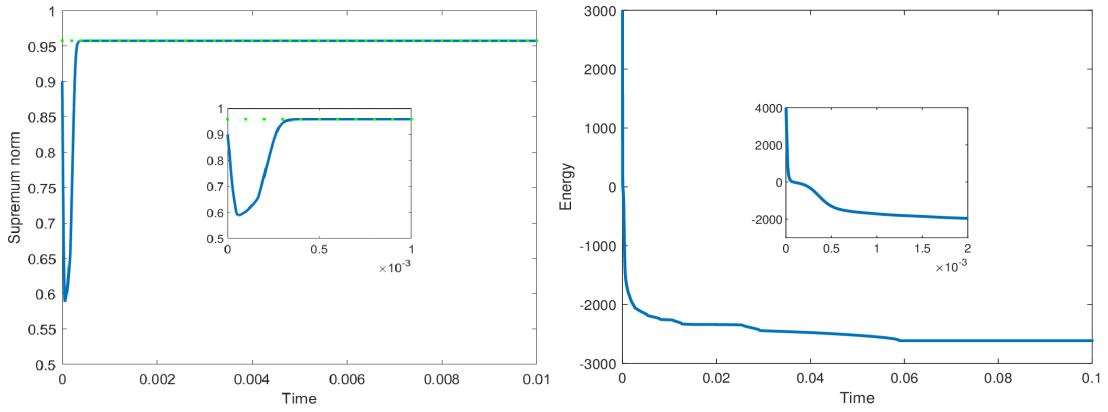

Figure 8: Evolutions of the supremum norm and the energy of numerical solution produced by the SII scheme for the Flory-Huggins potential case of the convective Allen-Cahn equation.

gular domain $[-1,1]^2$ with the mesh size h (It should be noted that the mesh size is not uniform due to the circular boundary). First, Tables 4 and 5 list the temporal and spatial convergence results for the double well potential case. It is easy to observe that the optimal convergence rates are achieved well. Then, Fig. 9 reports the numerical solutions for the double well potential case produced by SII scheme at $t=0.001,0.02$, and 0.05 and

Table 4: The temporal errors with the corresponding convergence rates of the SI, SII and SII-CN schemes on unit circular domain with the fixed mesh size $h=1/128$ ($T=0.01$).

	T/τ	$\|\cdot\|_\infty$	Rate	$\|\cdot\|_h$	Rate
SI scheme	64	1.1493e-02	–	9.7632e-03	–
	128	5.4612e-03	1.07	4.6481e-03	1.07
	256	2.3621e-03	1.21	2.0123e-03	1.21
	512	7.9102e-04	1.58	6.7421e-04	1.58
SII scheme	64	1.5564e-04	–	1.3110e-04	–
	128	3.9491e-05	1.98	3.3258e-05	1.98
	256	9.5281e-06	2.05	8.0234e-06	2.05
	512	1.9178e-06	2.31	1.6148e-06	2.31
SII-CN scheme	64	1.5564e-04	1.93	1.3110e-04	1.93
	128	3.9491e-05	1.98	3.3258e-05	1.98
	256	9.5283e-06	2.05	8.0235e-06	2.05
	512	1.9179e-06	2.31	1.6149e-06	2.31

Table 5: The spatial errors with the corresponding convergence rates of the SI scheme on unit circular domain with the fixed time step size $\tau=0.01$.

$1/h$	$\|\cdot\|_\infty$	Rate	$\|\cdot\|_h$	Rate
64	4.9128e-04	–	2.6847e-04	–
128	1.2652e-04	1.96	6.9207e-05	1.96
256	3.1921e-05	1.99	1.7689e-05	1.97
512	8.0072e-06	2.00	4.5872e-06	1.95

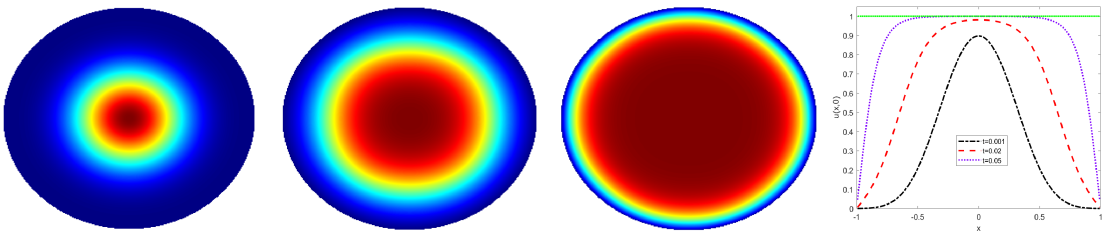

Figure 9: Numerical solutions produced by SII scheme at $t=0.001,0.02$, and 0.05 and their cross-sections with $y=0$ for the double well potential case of the convective Allen-Cahn equation on unit circular domain with $\tau=$1e-5 and $h=1/128$.

their cross-sections with $y=0$ where the green line $y=1$ gives the theoretical maximum bound, from which we can see that the MBP is well preserved.

Finally, we simulate the Flory-Huggins case on the unit circular domain. With the same parameter settings, the numerical solutions produced by SII scheme at t=0.001,0.02,

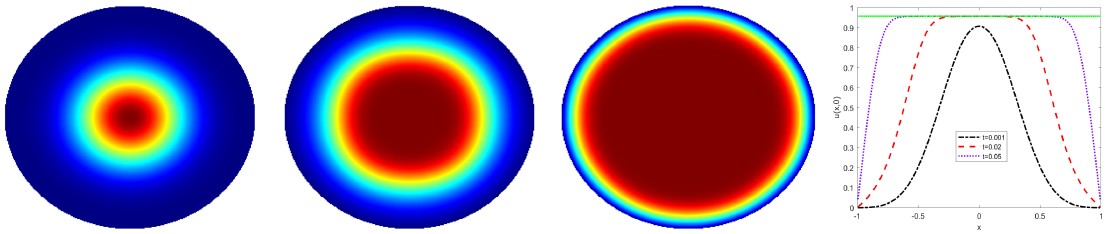

Figure 10: Numerical solutions produced by SII scheme at $t=0.001,0.02$, and 0.05 and their cross-sections with $y=0$ for the Flory-Huggins potential case of the convective Allen-Cahn equation on unit circular domain with $\tau=$1e-5 and $h=1/128$.

and 0.05 and their cross-sections with $y=0$ are plotted in Fig. 10 where the green line $y=0.9575$ gives the theoretical maximum bound. The discrete MBP is well preserved in this case again. All of these simulations confirm the robustness of the proposed schemes.

5.5 Three dimensional examples

We finally consider the three-dimensional convective Allen-Cahn equation. Again the SII scheme is used in all the following experiments. The nonlinear function is firstly taken as the double well potential (2.3). The velocity field is

$$\mathbf{v}(x,y,z,t)=e^{-t-x-y}[\cos(z),\cos(z),2\sin(z)]^{\top}.$$

The other parameter settings are $\tau=$1e-5, $h=1/128$, $\epsilon=0.01$. Fig. 11 gives the configurations of the numerical solutions at $t=0.001,0.01,0.07$ and 0.12. The corresponding

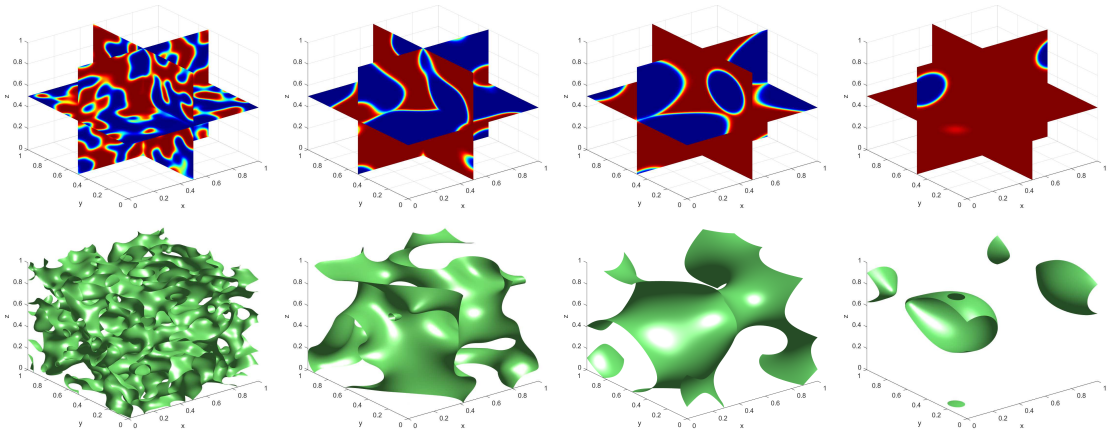

Figure 11: Numerical solutions produced by the SII scheme at $t=0.001,0.01,0.07$ and 0.12 (left to right) for the double well potential case of the convective Allen-Cahn equation in three dimensions. In each time panel, the top one represents the numerical solutions across the three central planes of the three dimensional cubic domain and the bottom one the isosurface.

developments of the supremum norm and the energy are plotted in Fig. 12 where the green line $y=1$ gives the theoretical maximum bound, which shows that the discrete MBP and the energy stability are numerically preserved.

We then consider the Flory-Huggins potential case (2.3) with $\theta=0.8$ and $\theta_c=1.6$. With the same parameters, Fig. 13 illustrates the configurations of the numerical solutions at $t=0.001,0.01,0.07$ and 0.12. The corresponding developments of the supremum norm and the energy are plotted in Fig. 14 where the green line $y=0.9575$ gives the theoretical maximum bound, which exhibits similar behaviors to those observed in the double well potential case.

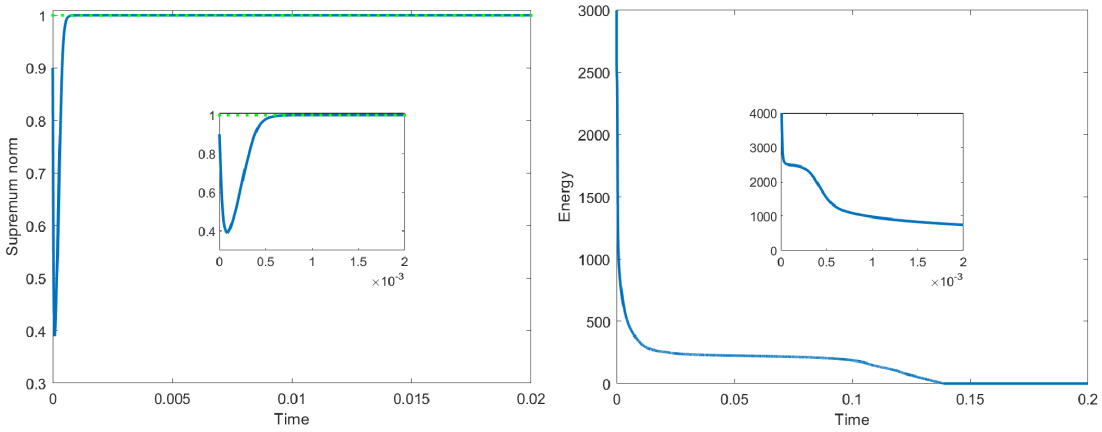

Figure 12: Evolutions of the supremum norm and the energy of numerical solution produced by the SII scheme for the double well potential case of the convective Allen-Cahn equation in three dimensions.

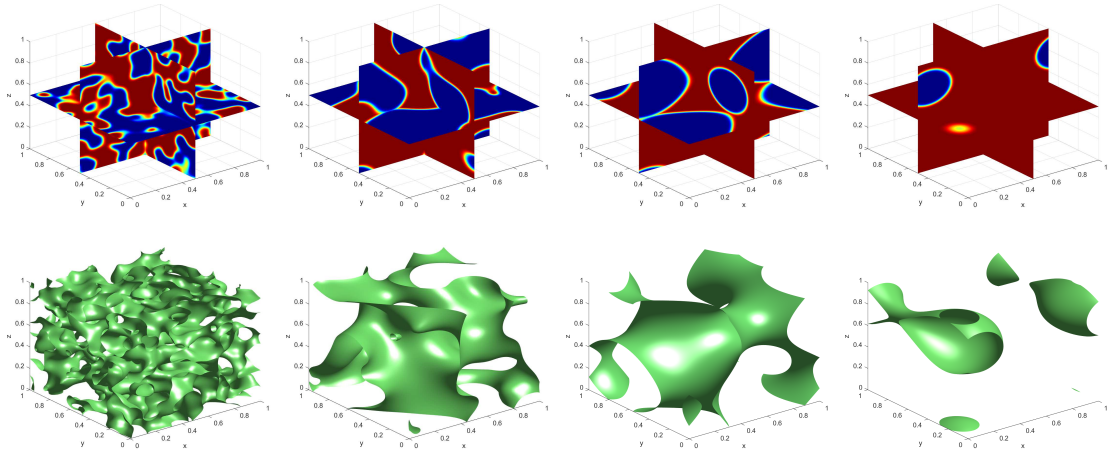

Figure 13: Numerical solutions produced by the SII scheme at $t=0.001,0.01,0.07$ and 0.12 (left to right) for the Flory-Huggins potential case of the convective Allen-Cahn equation in three dimensions. In each time panel, the top one represents the numerical solutions across the three central planes of the three dimensional cubic domain and the bottom one the isosurface.

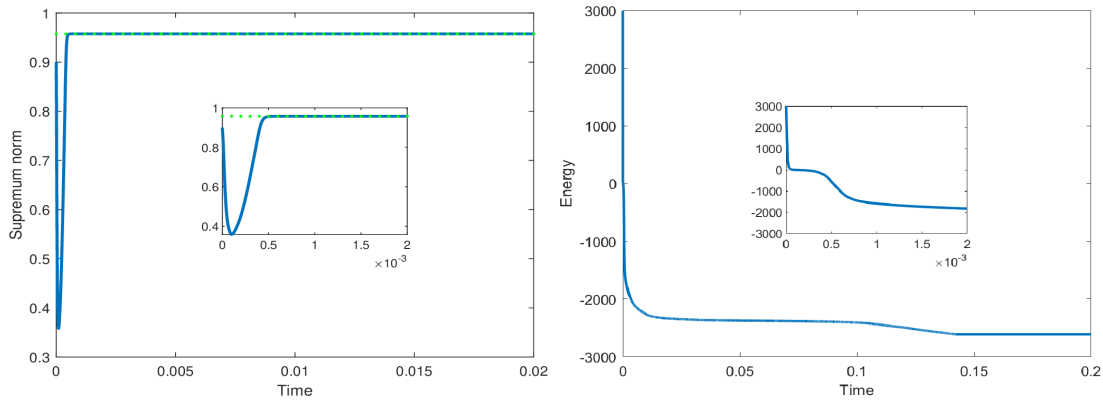

Figure 14: Evolutions of the supremum norm and the energy of numerical solution produced by the SII scheme for the Flory-Huggins potential case of the convective Allen-Cahn equation in three dimensions.

6 Concluding remarks

In this paper, we develop linear MBP-preserving numerical schemes for the convective Allen-Cahn equation, which are first- or second-order accurate in time. Unlike the classic upwinding strategy and the operator splitting method for treating the convective term, we combine the convective and diffusion terms into a single term with respect to a self-adjoint elliptic operator via an exponential transformation. This approach allows for quasi-symmetric discretization in space by the finite difference method with second-order accuracy. MBP and error estimates are rigorously analyzed for the proposed schemes. We also present numerical examples to confirm the theoretical results and demonstrate the efficiency of the proposed schemes. Our ongoing work includes fully discrete error analysis for the SII schemes as both the mesh size and the time step size approach zero, and application to coupled incompressible flows to design structure-preserving schemes.

Acknowledgements

J. Li's work is partially supported by the National Natural Science Foundation of China (Grant Nos. 12171216, 12301510 and 12526514). K. Wang's work is partially supported by the National Natural Science Foundation of China (Grant No. 12571417) and by the Natural Science Foundation of Chongqing (Grant No. 2024NSCQ-MSX0221).

References

[1] S. M. Allen and J. W. Cahn, *A microscopic theory for antiphase boundary motion and its application to antiphase domain coarsening*, Acta Metall., 27(6):1085–1095, 1979.

[2] M. Benes, V. Chalupecky, and K. Mikula, *Geometrical image segmentation by the Allen-Cahn equation*, Appl. Numer. Math., 51(2-3):187–205, 2004.

[3] M. Bessemoulin-Chatard, C. Chainais-Hillairet, and M. H. Vignal, *Study of a finite volume scheme for the drift-diffusion system. Asymptotic behavior in the quasi-neutral limit*, SIAM J. Numer. Anal., 52(4):1666–1691, 2014.
[4] Y. Cai, L. Ju, R. Lan, and J. Li, *Stabilized exponential time differencing scheme for the convective Allen-Cahn equation*, Commun. Math. Sci., 1(21):127–150, 2023.
[5] W. Chen, W. Feng, Y. Liu, C. Wang, and S. M. Wise, *A second order energy stable scheme for the Cahn-Hilliard-Hele-Shaw equations*, Discrete Contin. Dyn. Syst. Ser. B, 24(1):149–182, 2019.
[6] W. Chen, J. Jing, Q. Liu, C. Wang, and X. Wang, *Convergence analysis of a second order numerical scheme for the Flory-Huggins-Cahn-Hilliard-Navier-Stokes system*, J. Comput. Appl. Math., 450:115981, 2024.
[7] W. Chen, Y. Liu, C. Wang, and S. Wise, *Convergence analysis of a fully discrete finite difference scheme for the Cahn-Hilliard-Hele-Shaw equation*, Math. Comput., 85(301):2231–2257, 2016.
[8] W. Chen, C. Wang, X. Wang, and S.M. Wise, *Positivity-preserving, energy stable numerical schemes for the Cahn-Hilliard equation with logarithmic potential*, J. Comput. Phys.: X, 3:100031, 2019.
[9] A. E. Diegel, C. Wang, X. Wang, and S. M. Wise, *Convergence analysis and error estimates for a second order accurate finite element method for the Cahn-Hilliard-Navier-Stokes system*, Numer. Math., 137:495–534, 2017.
[10] J. Ding, C. Wang, and S. Zhou, *Convergence analysis of structure-preserving numerical methods based on Slotboom transformation for the Poisson-Nernst-Planck equations*, Commun. Math. Sci., 21(2):459–484, 2023.
[11] J. Ding, Z. Wang, and S. Zhou, *Positivity preserving finite difference methods for Poisson-Nernst-Planck equations with steric interactions: Application to slit-shaped nanopore conductance*, J. Comput. Phys., 397:108864, 2019.
[12] Q. Du, L. Ju, X. Li, and Z. Qiao, *Maximum principle preserving exponential time differencing schemes for the nonlocal Allen-Cahn equation*, SIAM J. Numer. Anal., 57(2):875–898, 2019.
[13] Q. Du, L. Ju, X. Li, and Z. Qiao, *Maximum bound principles for a class of semilinear parabolic equations and exponential time differencing schemes*, SIAM Rev., 63(2):317–359, 2021.
[14] Z. Du and T. Hou, *A linear second-order maximum bound principle preserving finite difference scheme for the generalized Allen-Cahn equation*, Appl. Math. Let.,158:109250, 2024.
[15] L. C. Evans, *Partial Differential Equations*, AMS, 1997.
[16] X. Feng X and A. Prohl, *Numerical analysis of the Allen-Cahn equation and approximation for mean curvature flows*, Numeri. Math., 94:33–65, 2003.
[17] X. Feng, H. Song, T. Tang, and J. Yang, *Nonlinear stability of the implicit-explicit methods for the Allen-Cahn equation*, Inverse Probl. Imag., 7(3):679–695, 2013.
[18] Y. Gao, D. Han, X. He, and D. Rude, *Unconditionally stable numerical methods for Cahn-Hilliard-Navier-Stokes-Darcy system with different densities and viscosities*, J. Comput. Phys., 454:110968, 2022.
[19] Y. Gao, X. He, L. Mei, and X. Yang, *Decoupled, linear, and energy stable finite element method for the Cahn-Hilliard-Navier-Stokes-Darcy phase field model*, SIAM J. Sci. Comput., 40(1):B110–B137, 2018.
[20] Y. Guo, C. Wang, S. Wise, and Z. Zhang, *Convergence analysis of a positivity-preserving numerical scheme for the Cahn-Hilliard-Stokes system with Flory-Huggins energy potential*, Math. Comput., 93(349):2185–2214, 2024.
[21] T. Hou and H. Leng, *Numerical analysis of a stabilized Crank-Nicolson/Adams-Bashforth finite difference scheme for Allen-Cahn equations*, Appl. Math. Let., 102:106150, 2020.
[22] T. Hou, D. Xiu, and W. Jiang, *A new second-order maximum-principle preserving finite difference*

scheme for Allen-Cahn equations with periodic boundary conditions, Appl. Math. Let., 104:106265, 2020.

[23] L. Isherwood, Z.J. Grant, and S. Gottlieb, *Strong stability preserving integrating factor Runge-Kutta methods*, SIAM J. Numer. Anal., 56(6):3276–3307, 2018.

[24] K. Jiang, L. Ju, J. Li, and X. Li, *Unconditionally stable exponential time differencing schemes for the mass-conserving Allen-Cahn equation with nonlocal and local effects*, Numer. Methods Part. Diff. Eq., 38(6):1636–1657, 2021.

[25] L. Ju, X. Li, Z. Qiao, and J. Yang, *Maximum bound principle preserving integrating factor Runge-Kutta methods for semilinear parabolic equations*, J. Comput. Phys., 439:110405, 2021.

[26] B. Kai, G. B. Hans, L. Tobias, and J. Christoph, *A maximum principle for drift-diffusion equations and the Scharfetter-Gummel discretization*, in: Scientific Computing in Electrical Engineering. Mathematics in Industry, Vol. 36, 45–52, 2021.

[27] J. Kim, *Phase-field models for multi-component fluid flows*, Commun. Comput. Phys., 12(3):613–661, 2012.

[28] L. Kovasznay, *Laminar flow behind a two-dimensional grid*, Math. Proc. Cambridge Philos. Soc., 44(1):58–62, 1948.

[29] R. Lan, J. Li, Y. Cai, and L. Ju, *Operator splitting based structure preserving numerical schemes for the mass conserving convective Allen-Cahn equation*, J. Comput. Phys., 472:111695, 2023.

[30] B. Li, J. Yang, and Z. Zhou, *Arbitrarily high-order exponential cut-off methods for preserving maximum principle of parabolic equations*, SIAM J. Sci. Comput., 42(6): A3957–A3978, 2020.

[31] J. Li, Y. Cai, R. Lan, L. Ju, and X. Wang, *Second-order semi-Lagrangian exponential time differencing method with enhanced error estimate for the convective Allen-Cahn equation*, J. Sci. Comput., 97:7, 2023.

[32] J. Li, L. Ju, Y. Cai, and X. Feng, *Unconditionally maximum bound principle preserving linear schemes for the conservative Allen-Cahn equation with nonlocal constraint*, J. Sci. Comput., 87(3):98, 2021.

[33] J. Li, X. Li, L. Ju, and X. Feng, *Stabilized integrating factor Runge-Kutta method and unconditional preservation of maximum bound principle*, SIAM J. Sci. Comput., 43(3):A1780–A1802, 2021.

[34] H. Liao, T. Tang, and T. Zhou, *A second-order and nonuniform time-stepping maximum-principle preserving scheme for time-fractional Allen-Cahn equations*, J. Comput. Phys., 414:109473, 2020.

[35] H. Liao, T. Tang, and T. Zhou, *On energy stable, maximum-principle preserving, second-order BDF scheme with variable steps for the Allen-Cahn equation*, SIAM J. Numer. Anal., 58(4):2294–2314, 2020.

[36] H. Liao, T. Tang, and T. Zhou, *An energy stable and maximum bound preserving scheme with variable time steps for time fractional Allen-Cahn equation*, SIAM J. Sci. Comput., 43(5):A3503–A3526, 2021.

[37] C. Liu and J. Shen, *A phase field model for the mixture of two incompressible fluids and its approximation by a Fourier-spectral method*, Physica D, 179(3-4):211–228, 2003.

[38] H. Liu and W. Maimaitiyiming, *Efficient, positive, and energy stable schemes for multi-D Poisson-Nernst-Planck systems*, J. Sci. Comput., 87:92, 2021.

[39] H. Liu and Z. Wang, *A free energy satisfying finite difference method for Poisson-Nernst-Planck equations*, J. Comput. Phys., 268:363–376, 2014.

[40] Y. Liu, W. Chen, C. Wang, and S. M. Wise, *Error analysis of a mixed finite element method for a Cahn-Hilliard-Hele-Shaw system*, Numer. Math., 135:679–709, 2017.

[41] A. Makki, A. Miranville, and M. Petcu, *A numerical analysis of the coupled Cahn-Hilliard/Allen-Cahn system with dynamic boundary conditions*, Int. J. Numer. Anal. Model., 19(5):630–655, 2022.

[42] G. Peng, Z. Gao, and X. Feng, *A stabilized extremum-preserving scheme for nonlinear parabolic equation on polygonal meshes*, Int. J. Numer. Meth. Fluids, 90:340–356, 2019.
[43] J. Shen, *Long time stability and convergence for fully discrete nonlinear Galerkin methods*, Appl. Anal., 38:201–229, 1990.
[44] J. Shen, T. Tang, and J. Yang, *On the maximum principle preserving schemes for the generalized Allen-Cahn equation*, Commun. Math. Sci., 14(6):1517–1534, 2016.
[45] J. Shen and X. Yang, *A phase-field model and its numerical approximation for two-phase incompressible flows with different densities and viscosities*, SIAM J. Sci. Comput., 32(3):1159–1179, 2010.
[46] J. Shen and X. Zhang, *Discrete maximum principle of a high order finite difference scheme for a generalized Allen-Cahn equation*, Commun. Math. Sci., 20(5):1409–1436, 2022.
[47] H. Song, L. Jiang, and Q. Li, *A reduced order method for Allen-Cahn equations*, J. Comput. Appl. Math., 292:213–229, 2016.
[48] T. Tang and J. Yang, *Implicit-explicit scheme for the Allen-Cahn equation preserves the maximum principle*, J. Comput. Math., 34(5):471–481, 2016.
[49] T. Tang, H. Yu, and T. Zhou, *On energy dissipation theory and numerical stability for time-fractional phase-field equations*, SIAM J. Sci. Comput., 41(6):A3757–A3778, 2019.
[50] X. Xiao, X. Feng, and J. Yuan, *The stabilized semi-implicit finite element method for the surface Allen-Cahn equation*, Discrete Contin. Dyn. Syst. Ser. B, 22(7):2857–2877, 2017.
[51] X. Xiao, R. He and X. Feng, *Unconditionally maximum principle preserving finite element schemes for the surface Allen-Cahn type equations*, Numer. Methods Partial Differential Equations, 36(2):418–438, 2020.
[52] X. Xu, L. Zhao, and C. Liu, *Axisymmetric solutions to coupled Navier-Stokes/Allen-Cahn equations*, SIAM J. Math. Anal., 41(6):2246–2282, 2010.
[53] J. Yang, Q. Du, and W. Zhang, *Uniform L^p-bound of the Allen-Cahn equation and its numerical discretization*, Int. J. Numer. Anal. Model., 15:213–227, 2018.
[54] J. Yang, Z. Yuan, and Z. Zhou, *Arbitrarily high-order maximum bound preserving schemes with cut-off postprocessing for Allen-Cahn equations*, J. Sci. Comput., 90:76, 2021.